Thermocline Forced by Annual and Decadal Surface Temperature Variation

Z. LIU

Atmospheric and Oceanic Science Program, Princeton University, Princeton, New Jersey

J. PEDLOSKY

Woods Hole Oceanographic Institution, Woods Hole, Massachusetts

(Manuscript received 16 January 1992, in final form 21 July 1993)

ABSTRACT

A two-layer thermocline model is modified by adding an essentially passive mixed layer above it. The surface temperature variation is simulated by a moving outcrop line. It is found that, in contrast to a surface wind stress, a surface temperature variation causes strong variability in the ventilated zone through subducted water, while it affects the shadow zone little.

Two types of buoyancy-forced solution are found. When the outcrop line moves slowly, the solutions are nonentrainment solutions. For these solutions, the surface heat flux is mainly balanced by the horizontal advection in the permanent thermocline. The mixed layer never entrains. The time-mean thermocline is close to the steady thermocline with the time-mean outcrop line.

When the outcrop line moves southward rapidly during the cooling season, the solutions become entrainment solutions. Now, deep vertical convection must occur because the horizontal advection in the permanent thermocline is no longer strong enough to balance the surface cooling. The time-mean thermocline resembles the steady thermocline with the early spring mixed layer, as suggested by Stommel. The local variability in the permanent thermocline is most efficiently produced by decadal forcings.

1. Introduction

Previous work on thermocline variability has emphasized the forcing of variable wind stress and the planetary waves excited at the oceanic eastern boundary (e.g., Anderson and Gill 1975). However, the surface buoyancy flux also exhibits strong variability at annual and decadal time scales, which is manifested by strong variability of surface temperature (or density if we assume a definite T–S relation) and mixed-layer depth. For instance, the annual surface temperature variation can be seen clearly in Figs. 1a,b (from Levitus 1982), which present the surface density of the World Ocean in spring and fall, respectively. The dot-connected lines mark the $24\sigma_t$ in the North Pacific and the $26\sigma_t$ in the North Atlantic. Both isolines vary from about 25° to 50° from spring to fall. This north–south migration distance is about the width of the subtropical gyres in both oceans. At the same time, the mixed-layer depth in the northern part of a subtropical gyre varies from 25 m in summer to more than 200 m in winter (Levitus 1982). These observations imply a strong variation of annual surface heat flux.

To date, few theories have been proposed to study the effect of a variable surface heat flux on the thermocline. One difficulty arises from the fact that the surface buoyancy flux influences the permanent thermocline through a mixed layer. Therefore, it is equally crucial to consider the dynamics of both the mixed layer and the thermocline on annual and decadal time scales. A deeper mixed layer can store more heat and therefore reduces the anomalous heat flux affecting the permanent thermocline. Hence, with a given surface buoyancy flux, the variability in the permanent thermocline depends heavily on the coupling between the mixed layer and the thermocline. Recently, the study of the coupling between the mixed layer and thermocline has concentrated on steady cases. Either the mixed layer is essentially passive (i.e., with the density and depth specified) (e.g., Pedlosky et al. 1984; Huang 1989; Wang 1990; Pedlosky and Robbins 1991) or the thermocline is somewhat specified (e.g., Marshall and Nurser 1991). The effect of a sloping mixed-layer depth has been emphasized as important in enhancing the ventilation effect. However, so far, no theory has been presented for time-dependent coupling.

This paper is an attempt toward understanding the coupling between a time-varying mixed layer and the permanent thermocline. The major issue addressed here is, How does the thermocline respond to a varying surface heat flux at annual and decadal time scales? As a first step, the surface buoyancy flux variation is represented by a variable surface temperature or density,

Corresponding author address: Dr. Zhengyu Liu, Princeton University, Sayer Hall, P.O. Box CN 710, Princeton, NJ 08544-0710.

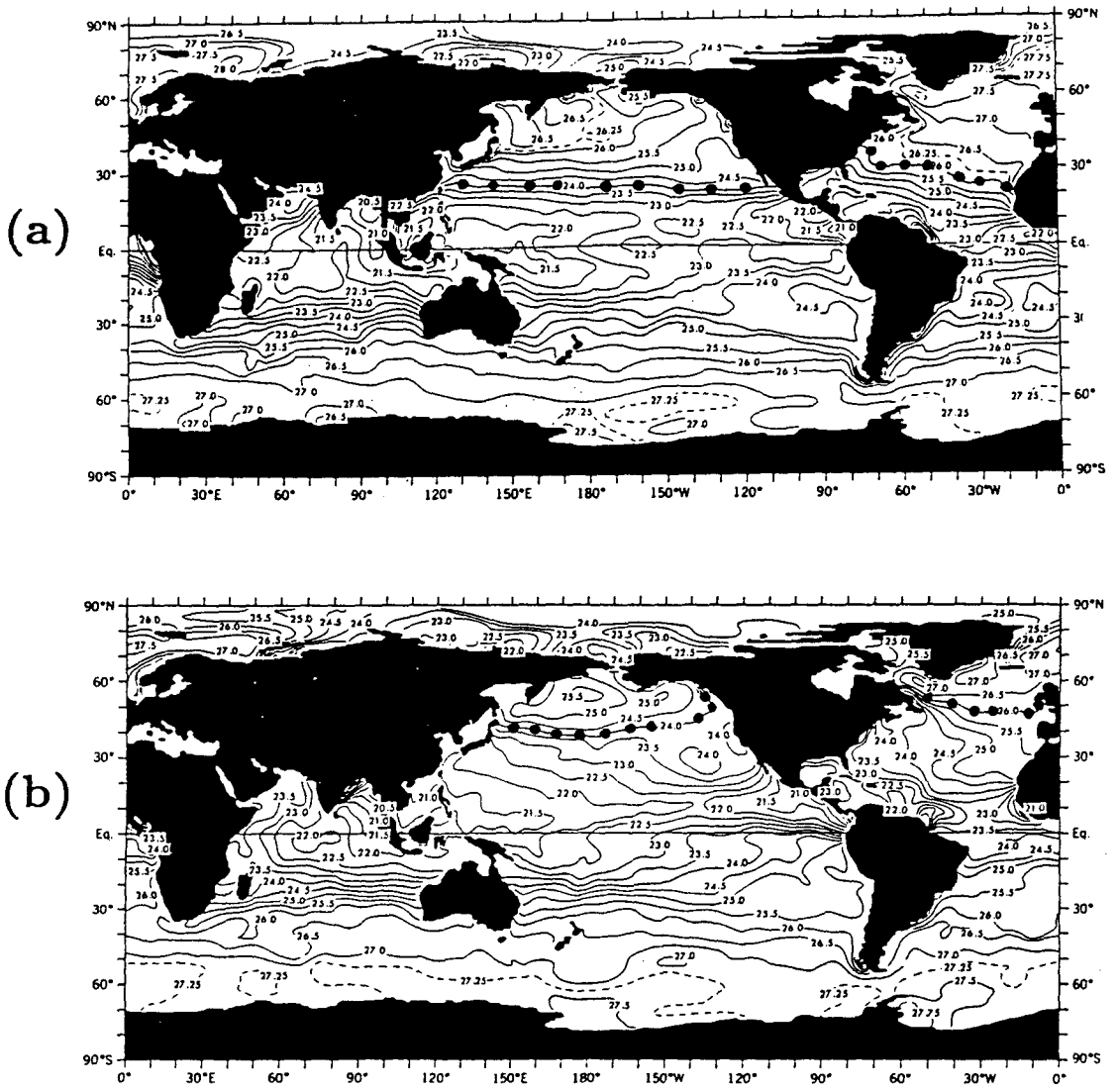

FIG. 1. The sea surface density [sigma-t (10^{-3} g cm^{-3})] for (a) the mean of February, March, and April and (b) the mean of August, September, and October. The dot-connected lines represent the 24 and 26 sigma-t lines in the North Pacific and North Atlantic, respectively (after Levitus 1982).

which in a layered model is equivalent to moving outcrop lines. To account for vertical convection, in section 2, a two-layer planetary geostrophic model is modified by adding a mixed layer on the top. The mixed layer is essentially passive in that the outcrop line and the mixed-layer depth are specified. Nevertheless, the velocity in the mixed layer is coupled with that in the thermocline through pressure. Section 3 considers the case with a slow outcrop line, which is produced by a weak surface heat flux. In the absence of a mixed layer, all solutions will be found gravitationally stable. For these solutions, the surface buoyancy flux anomaly is balanced by the horizontal temperature advection alone. Thus, no convection will develop. All the water subducts from the mixed layer into the thermocline, and there is no entrainment. Thus, these solutions will be called "nonentrainment solutions." However, if the surface cooling is very strong, the outcrop line may move southward faster than the particles near the surface. In that case, all solutions without a mixed layer become gravitationally unstable, implying the occurrence of deep convection. This is studied in section 4. In that case, it will be shown that stable solutions must have entrainment into the mixed layer. Thus, these solutions will be called "entrainment solutions." A convective scheme is developed to entrain waters into the mixed layer. In this way, stable solutions can be obtained. We will also discuss some features of the entrainment solution, which will be seen differing significantly from those of the

nonentrainment solution. Our major issue about thermocline variability is discussed in section 5. It is seen that the thermocline variability is determined by the subduction potential vorticities. For interannual and decadal flux anomalies, the variability increases its amplitude dramatically with period, implying that a decadal buoyancy forcing is efficient in forcing variability in the permanent thermocline.

Finally, the mixed layer deserves a further remark in its own right. Traditionally, the seasonal thermocline has been investigated with a 1D model (Turner and Kraus 1967; Kraus and Turner 1967; Warren 1972; Gill and Turner 1976; Niiler and Kraus 1977). However, in the area where the net annual buoyancy flux is large, a 1D model is likely to be no longer valid. Particularly in regions with net surface cooling, in a 1D model either the convection has to penetrate deeper and deeper or the surface temperature has to get colder and colder, because there is no other mechanism to balance this net buoyancy loss on the surface. Thus, on climate time scales, the locally unbalanced net heat flux should be balanced by horizontal advection (Woods 1985). Accordingly, in order to study the surface buoyancy effect on the basin-scale circulation at interannual time scales, it is essential to include horizontal advection as has been noted by Woods (1985). Since this paper concentrates on climate-scale variation, it is crucial to include the horizontal advection. This is indeed the case in our model, although the mixed layer in our model is crude and essentially passive. Our results thus may have important implications for the dynamics of the mixed layer.

2. A thermocline model with a time-dependent mixed-layer depth

To account for vertical convection in a subtropical gyre, one proper way is to add a mixed layer onto the thermocline. As shown in Fig. 2, our improved model has a mixed layer above the two-layer ideal fluid thermocline. The density and thickness of the upper layer are represented by ρ_1 and h_1, respectively. The density and thickness of the bottom layer are represented by ρ_2 and $h_2 = H - h_m - h_1$, respectively. The total depth of the model thermocline is H, which is chosen to be rigid and flat. The outcrop line is located at the latitude with the Coriolis parameter f_0. The density $\rho_m(x, f, t)$ in the mixed layer satisfies gravitational stability and equals the upper-layer density at the outcrop line; that is, $\rho_m \leqslant \rho_2$ for $f > f_0$, $\rho_m \leqslant \rho_1$ for $f < f_0$, and $\rho_m(x, f, t)|_{f=f_0(t)} \equiv \rho_1$; $h_m(x, f, t)$ is the mixed-layer depth.

To derive the equations, we first integrate a hydrodynamic equation in each layer to obtain the dynamic pressures

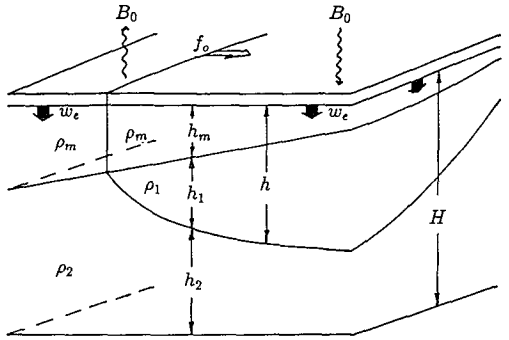

FIG. 2. Schematic figure of the model with one mixed layer and two ideal fluid layers. The model takes the thickness of the Ekman layer zero.

$$\frac{p_m}{\rho_m} \approx \frac{p_m}{\rho_0} = \gamma\eta + \gamma_m z \tag{2.1a}$$

$$\frac{p_1}{\rho_1} \approx \frac{p_1}{\rho_0} = \gamma\eta - \gamma_m h_m \tag{2.1b}$$

$$\frac{p_2}{\rho_2} \approx \frac{p_2}{\rho_0} = \gamma(\eta - h) - \gamma_m h_m, \tag{2.1c}$$

where ρ_0 is the mean density and

$$h = h_m + h_1,\ h + h_2 = H,$$

$$0 < \gamma_m(x, f, t) = \frac{\rho_1 - \rho_m(x, f, t)}{\rho_0} g,$$

$$\gamma = \frac{\rho_2 - \rho_1}{\rho_0} g = \text{const}; \tag{2.2}$$

η is the scaled surface elevation equivalent to the upper-layer pressure such that $\gamma\eta = \rho_0(p_{\text{surface}} + g\xi)$ where ξ is the surface elevation. In the mixed-layer pressure (2.1a), the first term is due to the pressure near the surface, while the second term is due to the variable density in the mixed layer. The outcropping condition is $h_1|_{f=f_0} = 0$, or

$$h|_{f=f_0} = h_m. \tag{2.3}$$

As a first step to study the effect of a variable surface heat flux, we specify the mixed-layer density ($\sim\gamma_m$) and depth (h_m), while we leave the mixed-layer velocity coupled with the thermocline through dynamic pressure. For basin-scale motions, the momentum equation in each layer reduces to the geostrophic balance

$$(u_m, v_m) = \frac{1}{f\rho_0}(-p_{my}, p_{mx})$$

$$(u_1, v_1) = \frac{1}{f\rho_0}(-p_{1y}, p_{1x})$$

$$(u_2, v_2) = \frac{1}{f\rho_0}(-p_{2y}, p_{2x}). \tag{2.4}$$

The remaining unknowns are η and h, which can be derived from the Sverdrup relation and potential vorticity conservation in the bottom layer. Now, the barotropic velocity is

$$\frac{\int_{-h_m}^{0} \mathbf{v}_m dz + h_1\mathbf{v}_1 + h_2\mathbf{v}_2}{H} \equiv \mathbf{v}_B = \frac{1}{f\rho_0}\mathbf{k}\times\nabla p_B. \quad (2.5a)$$

Then, the barotropic pressure can be found from (2.1), (2.4), and (2.5a) as

$$p_B = \frac{\rho_0}{2H\gamma}[2H(\gamma\eta - \gamma_m h_m) + \gamma_m h_m^2 + \gamma(H-h)^2]. \quad (2.5b)$$

The Sverdrup relation is $\beta(\int_{-h_m}^{0} v_m dz + h_1 v_1 + h_2 v_2) = fw_e$. Using (2.1), (2.4), and (2.5b) and assuming a flat bottom H = const, the Sverdrup relation can be integrated explicitly as

$$p_B = \rho_0\gamma D^2/2H + p_{\mathrm{BE}}, \quad (2.6a)$$

where

$$D^2 = 2f^2\int_0^x w_e dx/\beta\gamma, \quad p_{\mathrm{BE}} = p_{B|_{x=0}}, \quad (2.6b)$$

where the eastern boundary has been set at $x = 0$. Hereafter, the barotropic transport into the eastern boundary is assumed zero, or equivalently,

$$p_{\mathrm{BE}} = 0. \quad (2.6c)$$

The potential vorticity conservation in the bottom layer is $(\partial_t + \mathbf{v}_2\cdot\nabla)[f/(H-h)] = 0$. Substitution of (2.4) and (2.6) into this equation yields the equation for the depth $h = h_m + h_1$ as

$$h_t + \mathbf{v}_B\cdot\nabla h - \frac{1}{2Hf}J(\gamma_m h_m^2, h) - \frac{\beta}{2f^2}\left(1-\frac{h}{H}\right)(\gamma_m h_m^2 + \gamma h^2)_x = -\left(1-\frac{h}{H}\right)w_e. \quad (2.7)$$

Hereafter, the y coordinate will be changed to an f coordinate with the aid of $df = \beta dy$.

Now, we nondimensionalize equation (2.7). Superscripting a dimensional quantity by an asterisk, we have the nondimensional quantities

$$f = \frac{f^*}{f_n}, \quad \beta = \frac{\beta^*}{\beta_0}, \quad t = \frac{t^*}{T_W}, \quad x = \frac{x^*}{L}, \quad h = \frac{h^*}{H}, \quad w = \frac{w^*}{W}, \quad \gamma_m = \frac{\gamma_m^*}{\gamma^*}, \quad h_m = \frac{h_m^*}{H}. \quad (2.8)$$

In (2.8), W, f_n, β_0, H represent, respectively, the typical Ekman pumping velocity, the Coriolis parameter at the northern boundary of the subtropical gyre, the mean β value in a subtropical gyre, and the total depth. In addition, $T_W = H/W$, $\gamma = 2$ cm s^{-2}, $L = C_{\beta H} \times T_W$, and $C_{\beta H} = \beta_0 \times L_D^2 = \gamma H/f_n^2$, where L_D and $C_{\beta H}$ are the deformation radius and the typical midlatitude Rossby wave speed; T_W is then the advective time scale for a particle to sink to the bottom of the main thermocline. By Sverdrup relation, one can show that T_W is also the time scale for a particle driven by the wind to cross the basin; L is the zonal scale across which a midlatitude planetary wave travels in one advective time scale. If we choose the parameters as $W = 10^{-4}$ cm s^{-1}, $f_n = 2\Omega\sin(45°) = 10^{-4}$ s^{-1}, $H = 600$ m, and $\beta_0 = (2\Omega/a)\cos(35°) = 1.87\times10^{-13}$ s^{-1} cm^{-1}, it follows that $T_W \approx 20$ years, $L \approx 8400$ km, $C_{\beta H} \approx 1.6$ cm s^{-1}, and $L_D \approx 33$ km.

In the light of (2.8), (2.7) can be put in the dimensionless form:

$$h_t + \mathbf{v}_B\cdot\nabla h - \frac{1}{2f}J(\gamma_m h_m^2, h) - \frac{1}{2f^2}(1-h)(\gamma_m h_m^2 + h^2)_x = -(1-h)w_e, \quad (2.9a)$$

where by virtue of (2.5) and (2.6) the barotropic velocities are found to be

$$u_B = -\int_0^x (f^2 w_e)_f dx/f, \quad v_B\left(\equiv \frac{df}{ds}\right) = fw_e. \quad (2.9b)$$

Thus, the barotropic velocity is determined by the Sverdrup relation. Furthermore, for our essentially passive mixed layer h_m, γ_m will be specified. Thus, (2.9a) is a quasi-linear equation. For simplicity, we will adopt a special mixed layer whose density and depth are zonally independent; that is, $\partial x\gamma_m = \partial_x h_m = 0$. Equation (2.9a) then reduces to

$$h_t + \mathbf{v}_B\cdot\nabla h + \left[\frac{1}{2f}(\gamma_m h_m^2)_f - \frac{h(1-h)}{f^2}\right]h_x = -(1-h)w_e. \quad (2.10)$$

In particular, if the mixed layer vanishes, $h_m = 0$ (2.10) [or (2.9a)] degenerates to (for $h = h_1$)

$$h_t + \mathbf{v}_B\cdot\nabla h + C(h)h_x = -(1-h)w_e, \quad (2.11)$$

where $C(h) = -h(1-h)/f^2$ is the planetary wave speed. This is the equation for a two-layer model, which has been used by Liu (1993a,b) to study the effect of a variable Ekman pumping. Finally, we should point out that in (2.9) we have used the β-plane approximation (or a constant β).

3. Slow outcrop line case: Nonentrainment solutions

a. The solution

1) CHARACTERISTIC EQUATIONS

We start with the case of a slowly moving outcrop line. Now the surface cooling is weak, so one may ex-

pect that the convection is not strong. Therefore, we use the model without a mixed layer $h_m = 0$, that is, a two-layer planetary geostrophic model (2.11). The characteristic equations for (2.11) are

$$\frac{dt}{ds} = 1 \tag{3.1a}$$

$$\frac{df}{ds} = v_B = fw_e \tag{3.1b}$$

$$\frac{dh}{ds} = -(1-h)w_e(x,f,t) \tag{3.1c}$$

$$\frac{dx}{ds} = u_B(x,f,t) - h(1-h)/f^2$$

$$= -\left(f^2\int_0^x w_e dx\right)_f \Big/ f - h(1-h)/f^2. \tag{3.1d}$$

Here s is the distance from the initial time along a characteristic curve. It is linearly proportional to time. The initial conditions for characteristics are

$$(t,f,h,x)|_{s=0} = (t_i, f_i, h_i, x_i). \tag{3.2}$$

Division of (3.1b) and (3.1c) recovers the potential vorticity conservation along the characteristics

$$\frac{d}{ds}\left(\frac{f}{1-h}\right) = 0 \quad \text{or} \quad \frac{f}{1-h} = \frac{f_i}{1-h_i}. \tag{3.3}$$

Since our main interest is the surface buoyancy flux, the Ekman pumping will be set steady. For simplicity, the Ekman pumping is also taken to be zonally independent, or $w_e = w_e(f)$. Equation (3.1) can then be simplified as follows. First, (3.1a,b) are solved directly as

$$t = t_i + s \tag{3.4a}$$

$$s = \int_{f_i}^{f} d\mu/\mu w_e(\mu), \quad \text{or implicitly} \quad f = \hat{f}(f_i, s). \tag{3.4b}$$

Then, using potential vorticity conservation (3.3) to replace the h equation (3.1c) and noting the initial conditions in (3.2), we have the h solution in characteristic coordinates as

$$h = 1 - (1-h_i)f/f_i, \tag{3.4c}$$

where f is given in (3.4b). Finally, for the x equation, we use the differential form of (3.4b) $ds = df/fw_e(f)$ to replace the characteristic variable s by f in (3.1d). Then, noting (3.3), (3.1d) can be rearranged as

$$\frac{d}{df}[xf^2 w_e(f)] = -\frac{1-h_i}{f_i}h.$$

Substituting (3.4c) into the h on the right-hand side, the preceding equation can be integrated along the characteristics (thus, t_i, f_i, h_i, x_i are constants) to yield

$$2f^2 w_e(f)x = 2f_i^2 w_e(f_i)x_i + h^2 - h_i^2. \tag{3.4d}$$

The f and h are determined in (3.4b,c). Equations (3.4a–d) are the simplified version of characteristic equations. With proper initial conditions in (3.2), (3.4) will give the solution over the entire gyre.

2) VENTILATED ZONE

Since we will study periodically forced solutions after the initial adjustment, characteristics for the solution in the gyre start either from the outcrop line or the eastern boundary. [For a complete discussion of the solution of (3.1) including the initial adjustment period, the reader should refer to Liu (1991, 1993a).] The variation of sea surface density is simulated by the motion of an outcrop line. For simplicity, we adopt a zonal outcrop line varying with time; that is, $h|_{f=f_0} = 0$ and

$$f_0 = f_0(t). \tag{3.5}$$

This motion of the outcrop line can be thought of as caused by the net buoyancy effect or the combined surface and bottom buoyance effect on the mixed layer. If we want to derive a solution at a time t, all characteristics must start before this time; that is, $t_i \leqslant t$. Thus, with (3.5), characteristics originating from the outcrop line have the initial conditions

$$f_i = f_0(t_i), \quad h_i = 0. \quad t_i \leqslant t. \tag{3.6}$$

Substitution of (3.6) into (3.4a,b,c) yields the characteristic solution in its parametric form

$$f = \hat{f}[f_0(t_i), t - t_i] \equiv f^*(t, t_i), \quad \text{for} \quad t_i \leqslant t \tag{3.7a}$$

$$h = 1 - f^*(t,t_i)/f_0(t_i) \equiv h^*(t,t_i). \tag{3.7b}$$

In the special case when the outcrop line in (3.5) is steady, (3.7b) alone gives an explicit solution $h = 1 - f/f_0$, which is the solution for a steady ventilated zone in the two-layer model (see section 3 of Liu 1993a). For convenience, the solution (3.7) will be called the ventilated zone solution even with a moving outcrop line (3.5).

The physics of the parametric solutions $f^*(t, t_i)$ and $h^*(t, t_i)$ in (3.7) can be made clear as follows. At a time t, a lower-layer water column at a latitude f was subducted from the outcrop line at a previous time t_i:

$$t_i = \tau(f,t) \leqslant t, \quad \text{where} \quad f \equiv f^*[t, \tau(f,t)]. \tag{3.7c}$$

The interface depth at this latitude is $h = h^*[t, \tau(f, t)] \equiv h(f, t)$. Therefore, this water column always remembers its subduction time $\tau(f, t)$. It is important to notice that the subduction time is independent of the thermocline structure h in (3.7b). In fact, τ is determined by the $\hat{f}$ in (3.7a), which is derived from the f characteristic equation $df/ds = fw_e$. This equation is solely determined by the Ekman pumping and independent of h. Hence, during the evolution, each wa-

ter column in the lower layer remembers its subduction time and then can be labeled by the time according to (3.7a) or (3.7c) [independent of (3.7b)!]. In particular, at the latitude of the outcrop line $f = f_0(t)$, the water column is subducted at the present time $t_i = t$. In (3.7c), this suggests the identity $t \equiv \tau[f_0(t), t]$.

Figures 3a,b demonstrate schematically how the parameters for a water column are determined at latitude $f = F$ and time t. Since all subduction occurs before the present time t, the subduction time τ terminates at $\tau = t$ in Fig. 3a. In this case, the outcrop line moves so slowly that its southward velocity is never faster than the particle velocity or $0 > \dot{f}_0 > v_B(f_0)$. Therefore, no water column will be overtaken by a water column subducted later. In other words, at any time, the more north a water column is located, the later will be its subduction time, or equivalently, $\tau(f, t)$ increases monotonically with latitude as shown in Fig. 3a. Therefore, at each latitude F, the water column has a single subduction time $\tau(F, t)$. The labeling is done as follows. First, we find the subduction time for the water at latitude F from (3.7c) or (3.7a) as $\tau = \tau(F, t)$ as shown in Fig. 3a. Then, at latitude F, we find the depth of the interface from (3.7b) as $h = h^*[t, \tau(F, t)]$. Thus, at F, the water column has an interface at h^* and can be labeled by $\tau(F, t)$ as shown in Fig. 3b.

With (3.7b,c), one may note that the potential vorticity $q = f/(1 - h) = f/\{1 - h^*[t, \tau(f, t)]\}$ is constant on a latitude in the ventilated zone. This occurs because, first, the flat bottom and zonal outcrop line produce a constant subduction potential vorticity $q_s = f/(1 - h)|_{f=f_0} = f_0$, which is uniform along the outcrop line, and second, the meridional velocity in (3.2b) is also zonally independent [with $w_e = w_e(f)$]. The uniform subduction potential vorticity is advected southward. This produces a ventilated zone with a potential vorticity field, which is zonally uniform.

3) SHADOW ZONE

The solution (3.7) occupies only part of the basin. In the other part of the gyre, the solution is established by characteristics starting from the eastern boundary. For an eastern boundary interface depth $h_e(f, t)$ at $x = 0$, the initial conditions for these characteristics are $x_i = 0$, $h_i = h_e(f_i, t_i) = 0$, when $f_i \leqslant f_0(t_i)$ and $t_i \leqslant t$.

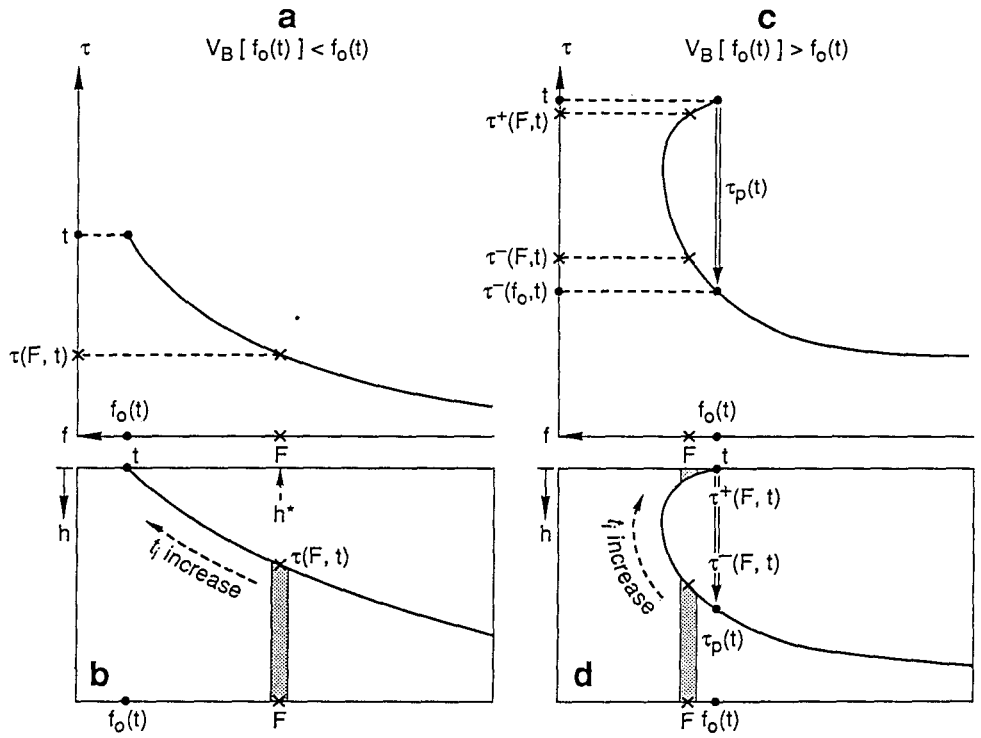

FIG. 3. The schematic figure showing how the interface solution is determined and labeled by the subduction time $\tau(f, t)$ at a given time t. (a) and (b) Slow outcrop line case. Panel (a) shows τ as a monotonic function of f because later water cannot catch up with an earlier subducted water; τ is single valued. Panel (b) shows the h^* profile, which is labeled by the subduction time according to (a). The h profile is stable. (c) and (d): Fast outcrop line case (during entraining stage). Now, because a later subducted water catches up with an earlier subducted water in (d), τ is double valued in (c), with the later branch τ^+ and the early branch τ^-. Corresponding to the double value τ function, the solution is unstable. Also shown schematically is the $\tau_p(t)$ function mapping, which gives the corresponding seasonally subducting time and determines the convective scheme used in (4.9a).

Here, for convenience, the depth of the eastern boundary interface has been set to zero. Thus, (3.4d) gives the solution

$$h^2 = 2f^2 w_e(f)x, \quad \text{when} \quad x > x_b(f, t). \quad (3.8)$$

The thermocline structure is independent of the outcrop line. Indeed, (3.8) is the same as the steady shadow zone solution in a two-layer model (Liu 1991, 1993a) except now the shadow zone boundary x_b varies with time. Therefore, the solution will still be called the shadow zone solution. The resemblance between (3.8) and the steady shadow zone is not surprising because the shadow zone does not feel the motion of the outcrop line except in the most western part where the characteristics starting from the outcrop line along the eastern boundary can arrive. The varying shadow zone boundary has the initial condition for characteristics as $x_i = 0$, $f_i = f_0(t_i)$, $h_i = 0$. Thus, (3.4) gives the parametric form of x_b

$$x_b^*(t, t_i) \equiv \frac{(h^*)^2}{2(f^{*2} w_e(f^*)}, \quad (3.9)$$

where f^*, h^* are given in (3.7a,b).

b. *Nonentrainment solutions*

Equations (3.7), (3.8), and (3.9) form the solution in the entire gyre. As an example, we take a spatially uniform Ekman pumping

$$w_e(f) = W_0 = \text{const} < 0. \quad (3.10)$$

(This Ekman pumping function will be used for all the calculations.) With (3.10), (3.4b) gives the f characteristic solution

$$f = f_i e^{W_0 s} \equiv \hat{f}(f_i, s). \quad (3.11)$$

With an outcrop line $f_0(t)$, the parametric solution in the ventilated zone is derived from (3.11), (3.7a), and (3.7b) as

$$f = f^*(t, t_i) = f_0(t_i) e^{W_0(t-t_i)} \quad (3.12a)$$

$$h = h^*(t, t_i) = 1 - e^{W_0(t-t_i)}. \quad (3.12b)$$

Since observations show that the annual surface temperature varies nearly harmonically, the outcrop line will be assumed harmonically oscillating as

$$f_0(t) = f_g(1 + a\cos\omega t), \quad 0 \leqslant a \leqslant 1, \quad (3.13a)$$

where f_g is the mean position of $f_0(t)$, and af_g is the amplitude of the oscillation. The most northern and southern latitudes of the outcrop line are, respectively,

$$f_{0\max} = f_g(1 + a) \text{ and } f_{0\min} = f_g(1 - a), \quad (3.13b)$$

which are reached by the outcrop line f_0 at the times

$$t = p_n \equiv 2n\pi/\omega \quad \text{and} \quad t = p_n + \pi/\omega, \quad (3.13c)$$

where n is an integer. In the case of an annual period, these two times correspond to about September and March (since the sea surface temperature lags the surface heat flux about 90° in phase). For a thermocline depth of about 600 m, the scaling in (2.8) suggests that the time scale is $T_w = H/W_e \sim 20$ years. Therefore, a nondimensional annual frequency is about $\omega \approx 100$, while a decadal frequency is about $\omega \approx 10$. Without confusion, the 12 months will still be used to refer to relative times in the oscillation even for periods other than the annual period.

Figure 4 displays an example of weak decadal forcing, with $W_0 = -1$ in (3.10) and $f_g = 0.7$, $\omega = 5$, $a = 0.19$ in (3.13a). Along $x = -1$, the meridional profiles at $\omega t = 0$, $\pi/2$, π and $3\pi/2$, corresponding to September, December, March, and June, are presented in Figs. 4a–d. The northern part that deepens southward is the ventilated zone in (3.7a,b), while the southern part that shallows southward is the shadow zone in (3.8). Several features are interesting. First, the interface slope near the surface is small at September (Fig. 4a), implying a strong stratification. As the outcrop line moves southward due to cooling, the slope steepens but remains stable (Fig. 4b) with the maximum slope (or a minimum stratification) achieved a little before March. Later, the outcrop line returns northward due to heating. The thermocline responds with a quick decrease in the slope or a rapid buildup of the stratification (Figs. 4c,d). The second feature is the relation between the time-mean thermocline profile and some steady thermocline profiles. In Fig. 4e, the time-mean interface $\langle h \rangle$ is depicted as the dot-connected line, while the short and long dashed lines, respectively, draw the steady LPS solutions with the outcrop line at the time-mean position (f_g) and southernmost position ($f_{0\min}$) (March). It is seen that the time-mean profile is very close to the steady thermocline with the mean outcrop line (except for the very northern part). Third, the variability in the permanent thermocline is strong as shown by a local time series of h in Fig. 4f. Although the outcrop line (3.13a) is harmonic, the interface variation is not! It has a relatively slow deepening and a rapid rise and therefore possesses strong superharmonics in the power spectrum (or Fourier series) of the h time series as presented in Fig. 4g. This power spectrum differs significantly from that produced by a wind forcing. In the wind forcing case, discussed by Liu (1993b), the time-mean component is comparable to the second superharmonic while other higher superharmonics are negligible. In contrast, now, the time-mean component is smaller than most superharmonics (Fig. 4g).

These features are also observed clearly in Fig. 5a, where the zonal profiles are displayed. Furthermore, the shadow zone boundary x_b at the four seasons is drawn in Fig. 5b. In the region swept through by x_b, the shadow zone and ventilated zone dominate alternately. [A similar phenomenon has been seen with a

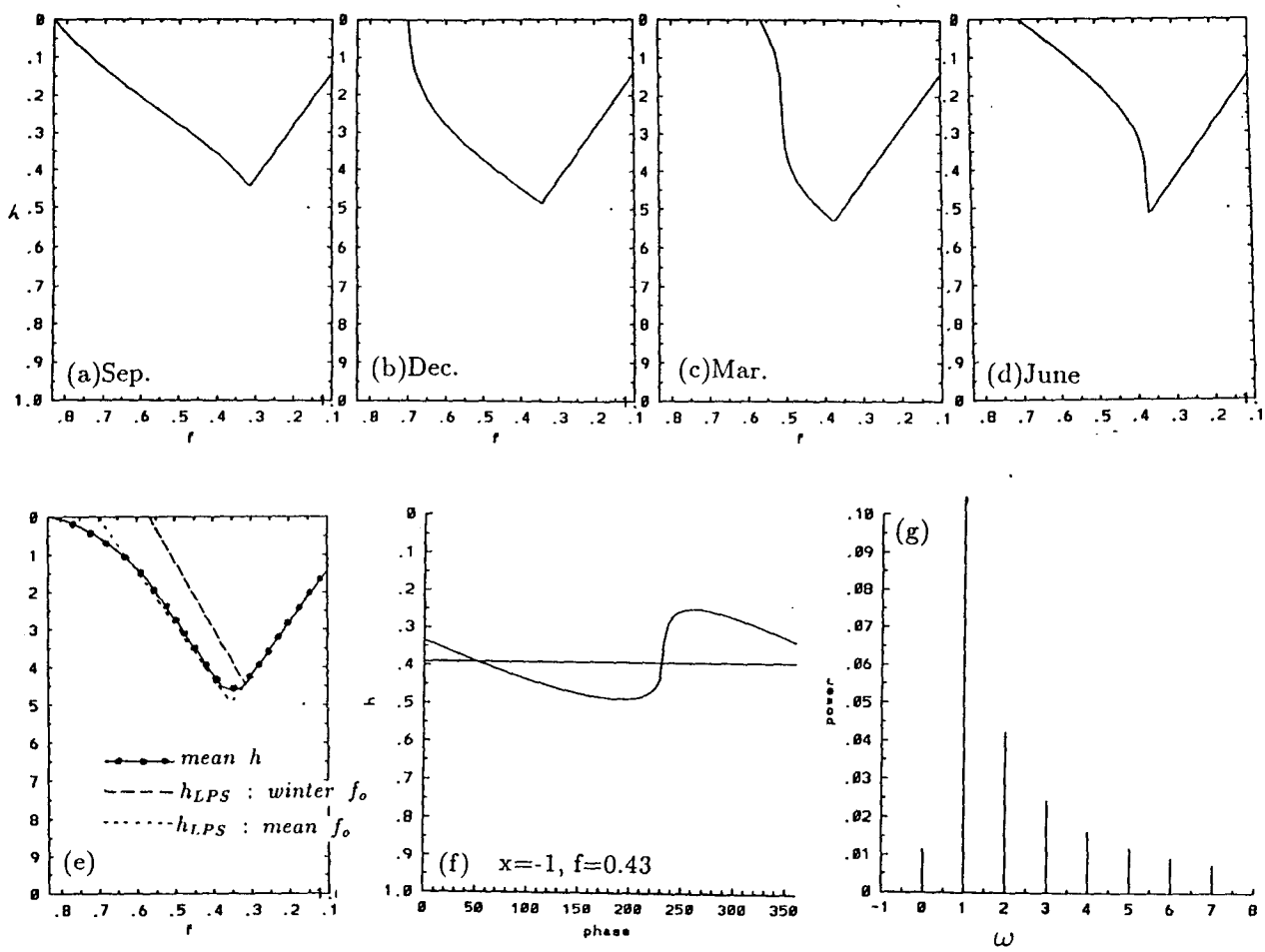

FIG. 4. The nonentrainment solution in the absence of a mixed layer; $w_e(f) = -1, f_0(t) = f_g[1 + a\cos(\omega t)]$, $\omega = 5$, $a = 0.19, f_g = 0.7$. (a)–(d) The meridional sections along $x = -1$ in September ($\omega t = 0$), December ($\omega t = \pi/2$), March ($\omega t = 0$), and June ($\omega t = 0$), respectively. (e) The time-mean profile (dot connected line), the steady LPS thermocline with the time-mean outcrop line (short dash line), and the steady LPS thermocline with the outcrop line in March. (f) Local time series of interface during one period. (g) Fourier components of the local time series in (f).

variable wind forcing in an alternative zone (Liu 1993a,b).]

The solution above is an example of *nonentrainment solution,* which remains stable without a variable mixed-layer depth. It is so named because of the absence of entrainment, as will be shown later. However, if the amplitude or frequency increases further (so that df_0/dt increases), the solution may exhibit gravitational instability. Figures 6a–d show a solution with the same frequency as that in Fig. 4 and Fig. 5 but with a larger amplitude of $a = 0.4$ (the shadow zone part of the solution is not shown in Fig. 6). During winter, when the outcrop line moves southward rapidly, the solution becomes gravitationally unstable. Later, a bulb of unstable water is advected downward and southward. An annual frequency case is shown in Figs. 6e–h. The profile has many more unstable pulses of waters because of the higher frequency. These two solutions are not physically valid because of the instability. Before finding stable solutions under fast outcrop lines such as those in Fig. 6, we first study the criterion for the breakdown of the nonentrainment solution.

c. *The criterion for the breakdown of nonentrainment solutions*

Obviously, a gravitationally stable solution must have a stable slope of interface

$$\partial_f h \leqslant 0 \quad \text{everywhere.} \tag{3.14a}$$

Inside the ventilated zone of our two-layer model, when the potential vorticity does not vary along a latitude it holds that $\partial_x h = 0$ or $Ch_x = 0$ in (3.7) south of the outcrop line. Thus, there is no Rossby wave effect and the associated nonlinear steepening term vanishes. Then, we speculate that gravitational instability can only be caused on the outcrop line. (This has been seen as true in all the numerical experiments, but we

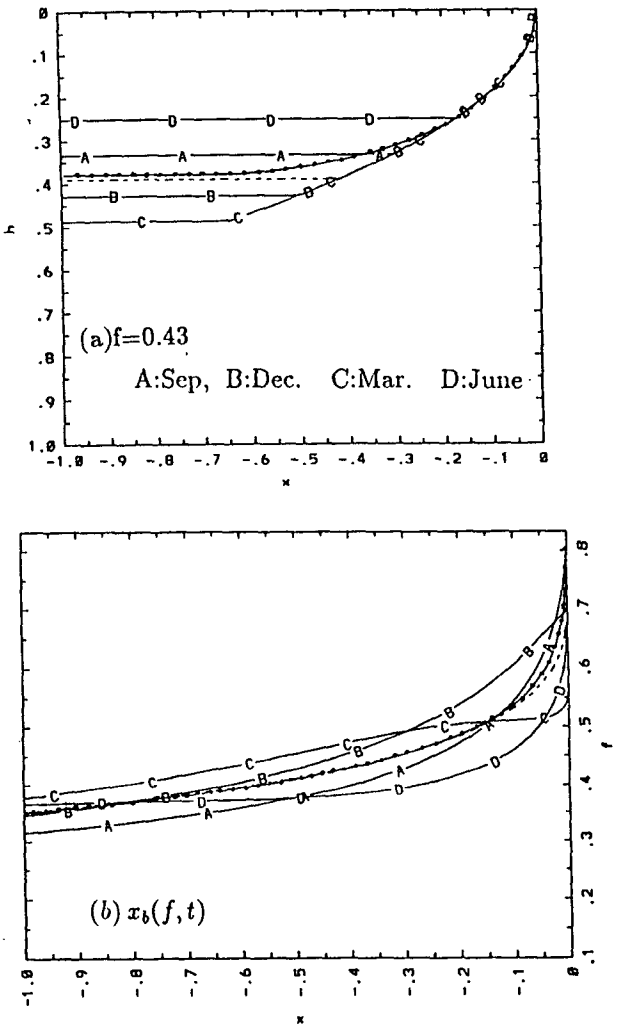

FIG. 5. The zonal sections and shadow zone boundaries of the example in Fig. 4. (a) Zonal sections at four seasons. The dot-connected line is the time-mean profile. The short dash line is the steady LPS thermocline with the time-mean outcrop line. (b) Similar to (a) but for the shadow zone boundary.

are unable to prove it mathematically.) Thus, (3.14a) is equivalent to

$$\partial_f h|_{f=f_0(t)} \leq 0 \quad \text{for all } t. \tag{3.14b}$$

This slope can be derived from the mass balance of the upper layer near the outcrop line. Let us take a small volume near the outcrop line in the upper layer with a δf length on its top and a δh thickness on its southern side; $-w_e\delta f$ is the downward mass flux from the top and $(v_B - \dot{f}_0)\delta h$ is the southward mass flux through the southern side (since the outcrop line is moving with the speed $\dot{f}_0$, the mass flux through the southern side is caused by the relative velocity $v_B - \dot{f}_0$). Noting the absence of mass flux across the interface on the northern and bottom side, the mass balance for the small volume is then

$$-w_e\delta f = [v_B(f_0) - \dot{f}_0]\delta h \quad \text{near } f_0, \tag{3.15a}$$

where $\dot{f}_0 \equiv df(t)/dt$. Equation (3.15a) is equivalent to

$$\left.\frac{\partial h}{\partial f}\right|_{f=f_0} = \frac{-w_e}{v_B(f_0) - \dot{f}_0}. \tag{3.15b}$$

This slope can also be derived mathematically as in appendix A. With the aid of (3.15b), (3.14b) becomes

$$\partial_f h|_{f=f_0} = \frac{-w_e(f_0)}{v_B(f_0) - \dot{f}_0} \leq 0. \tag{3.16}$$

In a subtropical gyre, $w_e \leq 0$. Thus, when the outcrop line remains slower than the southward barotropic flow $v_B - \dot{f}_0 < 0$, the slope (3.16) is always stable, implying the absence of convection or entrainment. Thus, these solutions will be called nonentrainment solutions:

nonentrainment solution:

$$v_B[f_0(t)] - \dot{f}_0(t) \leq 0 \quad \text{for all } t. \tag{3.17}$$

For a nonentrainment solution, a subducted water column will never be caught by water subducted later. Thus, the farther north a water column is located, the later is its subduction time. In other words, the water column of layer 2 at a latitude f consists solely of the water injected from the outcrop line at a single time $\tau(f, t)$ (see Fig. 3b). This suggests that the subduction time τ is single valued with respect to f, as depicted schematically in Fig. 3a. This can also be proven mathematically. With the aid of (3.7a) and (3.4a,b), we have

$$t - t_i = \int_{f_0(t_i)}^{f^*(t,t_i)} d\mu / v_B(\mu).$$

Differentiating this equation with respect to t_i yields

$$\partial_{t_i} f^*|_{t\,\text{fixed}} = -\frac{v_B(f^*)}{v_B(f_0)}[v_B(f_0) - \dot{f}_0]. \tag{3.18}$$

If $v_B - \dot{f} < 0$ always holds as in (3.17), $\partial_{t_i} f^* > 0$ is always true. From (3.7c) we then have $\partial f \tau = 1/\partial_{t_i} f^* > 0$. Thus, the subduction time increases monotonically with latitude. Condition (3.17) is marginally satisfied by the solution in Fig. 4 and Fig. 5.

If (3.17) is violated, the solution will exhibit an unstable slope as shown in examples of Fig. 6, implying the occurrence of cold convection or entrainment. The solutions will then be called an entrainment solution; that is,

entrainment solution:

$$v_B[f_0(t)] - \dot{f}_0(t) > 0 \quad \text{at some } t. \tag{3.19}$$

The two examples in Fig. 6 can be checked to satisfy (3.19). For an entrainment solution, at a time when the southward speed of the outcrop line is faster than the particle speed, newly injected waters will catch up with previously injected waters left behind (north of)

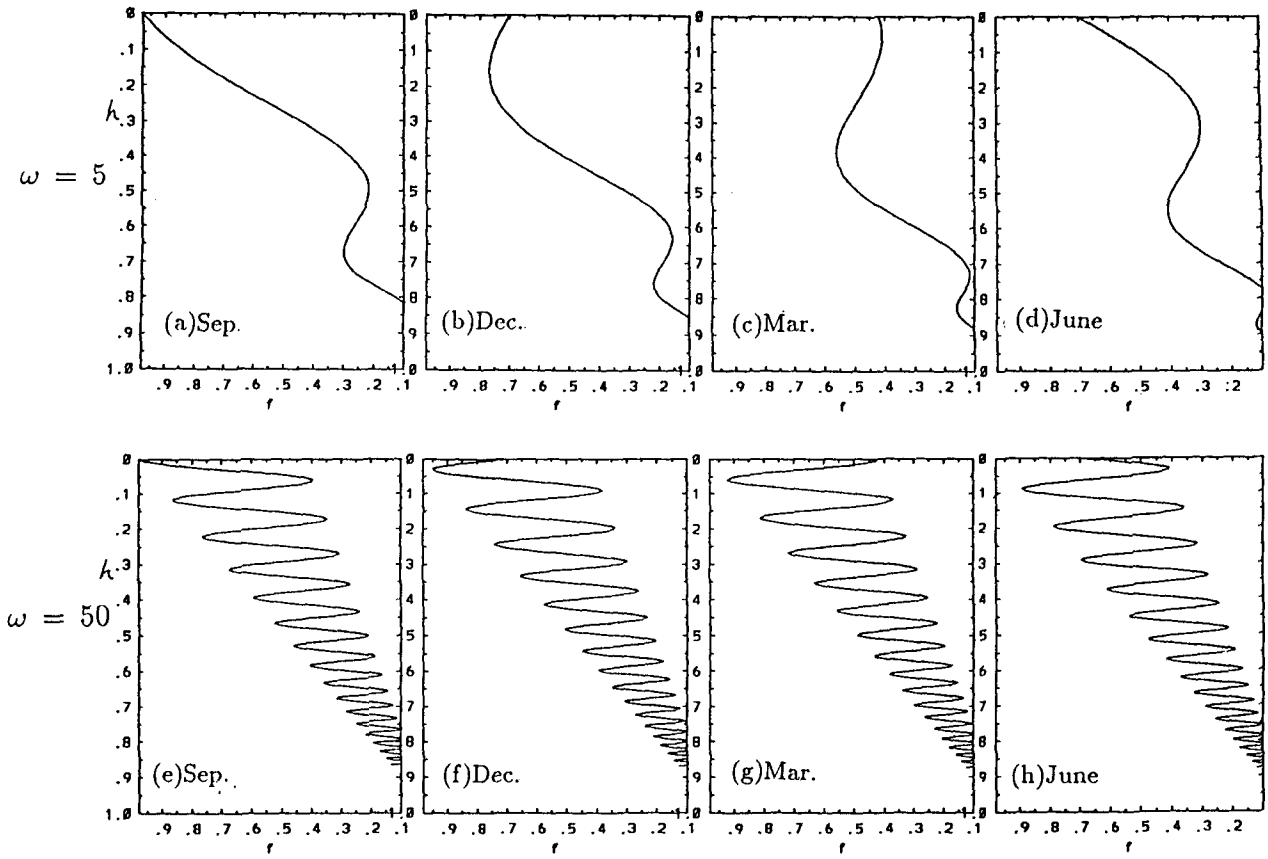

FIG. 6. Unstable entrainment solutions. (a–d) Meridional sections at four seasons with the same parameter as in Fig. 4 except $a = 0.4$. Only the ventilated zone solution is drawn. (e–h) Same as in (a–d) except for $\omega = 50$.

the outcrop line. Equation (3.18) shows that now $\partial_{t_i} f^* < 0$ or $\partial_f \tau < 0$. Thus, $\partial_f \tau$ changes sign and τ has a double value at latitudes north of the outcrop line. This case is shown schematically in Figs. 3c,d. We will denote the later and earlier branches of τ as τ^+ and τ^-, respectively (Fig. 3c). Correspondingly in Fig. 3d, a water column subducted at $\tau^+(F, t)$ now overlies the water column subducted at an earlier time $\tau^-(F, t)$, implying a gravitationally unstable solution as shown in (3.16).

The unstable structure suggests the occurrence of cold convection near the surface. The physics can be understood as follows. Intuitively, one may think that a slow outcrop line in (3.17) is produced by a weak surface cooling (in the cooling period) while a fast outcrop line in (3.19) is forced by a strong surface cooling. [This can be proven as in appendix A of chapter 4 in Liu (1991).] Now, we consider an ideal fluid thermocline. If we impose a temporal surface cooling uniformly over the surface of the whole gyre, the surface temperature, and then the temperature of the whole water column, should decrease. If the stratification is stable, in a subtropical gyre, the downward vertical velocity always tends to warm the water column. Thus, the only mechanism to balance the surface cooling is a cold horizontal advection. This is the case of a non-entrainment solution. However, since the meridional velocity v is largely determined by the Sverdrup relation, there is no frontogenesis mechanism under the uniform surface cooling. As a result, the horizontal cold advection cannot grow very strong. Therefore, if the surface cooling is too strong, the horizontal cold advection may not be able to balance the cooling. On the other hand, the downward vertical velocity is still forced by the surface Ekman pumping in the subtropical gyre. Thus, the only way to balance the strong surface cooling is to have an unstable stratification near the surface that, together with the downward velocity, tends to cool the water column. This is the case of entrainment solution (see examples in Figs. 3c,d and Fig. 6). Of course, these unstable solutions are not physically valid. Indeed, the unstable stratification implies a cold convection near the surface, which produces a near-neutral stratification or a mixed layer.

4. Fast outcrop line case: Entrainment solutions

a. The solution

As seen above, when the outcrop line moves southward rapidly, a two-layer model gives gravitationally unstable solutions. This suggests the occurrence of deep convection. For these cases, one may expect that the mixed layer becomes crucial. Therefore, model (2.10) will be used. Comparing (2.10) with (2.11), we see that their characteristic equations are the same in (3.1a,b,c) except the x characteristic equation (3.1d). The x equation is changed by the zonal thermal wind, which is produced by the meridional variation of the mixed layer. Therefore, the simplified equations (3.4a,b,c) are also characteristic equations for (2.10) [although one should note that in (2.10), $h = h_1 + h_m$, while in (2.11) $h = h_1$ due to $h_m = 0$].

Hereafter, we will focus on the solution in the ventilated zone, which is established by characteristics originating from the outcrop line. Thus, the characteristic solutions are determined in (3.4a,b,c) and the x characteristic equation of (3.4d). Then, from (2.3), the initial conditions for characteristics are

$$f_i = f_0(t_i), \quad h_i = h_m[f_0(t_i), t_i] \equiv H_m(t_i). \tag{4.1}$$

Here H_m is the depth of the mixed layer under the outcrop line. Substituting (4.1) into (3.4a,b,c) yields the solution in the ventilated zone as

$$f = \hat{f}[f_0(t_i), t - t_i] \equiv f^*(t, t_i) \tag{4.2a}$$

$$h = 1 - [1 - H_m(t_i)]f^*(t, t_i)/f_0(t_i) \equiv h^*(t, t_i). \tag{4.2b}$$

Equation (4.2) is the generalized solution of (3.7). Its physics can also be explained similarly to that of (3.7). That is, each water column remembers its subduction time

$$t_i = \tau(f, t) \leqslant t, \quad \text{where} \quad f \equiv f^*[t, \tau(f, t)]. \tag{4.2c}$$

Since (4.2a) is exactly the same as (3.7a), the subduction (4.2c) is the same as (3.7c). Because (4.2) determines the solution in the ventilated zone completely, we do not need to resort to the x characteristic equation.

Similar to (3.7b,c), (4.2b,c) show that the h solution or potential vorticity is independent of x if the mixed-layer depth is zonally independent $\{h = h^*[t, \tau(f, t)]\}$. The physical reason is similar to the case of (3.7b,c). Then, in the ventilated zone, (2.10) becomes

$$h_t + v_B h_f = -(1 - h)w_e, \quad f < f_0(t).$$

With the outcropping condition (4.1), this gives perhaps the simplest model accounting for subduction under a variable mixed-layer depth. We see that the horizontal buoyancy advection in the thermocline is simple. The flow field is known from the Sverdrup relation and therefore is independent of the buoyancy effect. As a result, our problem is greatly simplified.

Equations (4.2a,b) give the parameteric solution (for the ventilated zone) of (2.10). However, the solution may not be gravitationally stable for an arbitrarily specified $f_0(t)$ and $H_m(t)$. One example we have seen is the case with a vanishing mixed-layer depth $H_m(t) = 0$. For this case, if the outcrop line moves southward faster than the particle velocity $\dot{f}_0 < v_B < 0$, the solution becomes unstable as shown by examples in Fig. 6 and in equation (3.16). Therefore, we need to find some constraints on the depth of the mixed layer, under which solution (4.2) remains stable. The necessity for these constraints is not totally surprising. This is because the mixed layer here is partially coupled with the thermocline through pressure. Consequently, the behavior and structure of the mixed layer can not be specified completely arbitrarily.

1) A STABLE SLOPE: RESTRAINING THE PENETRATION OF THE MIXED LAYER

First of all, it is obvious that a stable solution must have a stable slope all the time in the gyre; that is, $\partial_f h \leqslant 0$ *everywhere* as in (3.14a). With an argument similar to that for (3.14b), this seems to be equivalent to a stable slope at the outcrop line $\partial_f h|_{f=f_0} \leqslant 0$. Similar to (3.16), this slope can also be derived by the mass balance of layer 1 near the outcrop line as

$$-w_m^* \delta f = [v_B(f_0) - \dot{f}_0]\delta h, \tag{4.3a}$$

or

$$\partial_f h|_{f=f_0(t)} = \frac{-w_m^*}{v_B[f_0(t)] - \dot{f}_0(t)}, \tag{4.3b}$$

where w_m^* is the mass entrainment velocity at the bottom of the mixed layer near the outcrop line. From the continuity equation, we have w_m^*,

$$w_m^* = \frac{dH_m}{dt} + w_m, \tag{4.4a}$$

where $w_m = w|_{z=-H_m}$ is the vertical velocity at the bottom of the mixed layer at the outcrop line and can be proven to be (see appendix A)

$$w_m = (1 - H_m)w_e(f_0). \tag{4.4b}$$

With a vanishing $H_m = 0$, (4.4a,b) show that $w_m^* = w_e$. Thus, (4.3a,b) degenerate to (3.15a,b).

Hence, a stable slope requires $\partial_f h|_{f=f_0(t)} = -w_m^*/[v_B(f_0) - \dot{f}_0] \leqslant 0$, *for all* t, or

$$0 > w_m^* \quad \text{when} \quad v_B(f_0) - \dot{f}_0 < 0, \tag{4.5a}$$

$$0 < w_m^* \quad \text{when} \quad v_B(f_0) - \dot{f}_0 > 0. \tag{4.5b}$$

Equation (4.5a) states that, when the outcrop line moves southward less rapidly than the particle, water mass subducts from the mixed layer into the thermocline. On the other hand, (4.5b) says that during the time interval when the outcrop line moves southward more rapidly

than the particle, the mixed layer must be entrained from the thermocline below. The time interval during which (4.5b) is satisfied is therefore called the *entraining stage.* For a periodically moving outcrop line in (3.13), the entraining stage is

entraining stage:

$$\tau_1^n \leqslant t \leqslant \tau_2^n, \tag{4.6a}$$

where $p_n \leqslant \tau_1^n, \tau_2^n \leqslant p_{n+1}$ with $p_n = 2n\pi/\omega$ [see (3.13c)]. Here n refers to the entraining stage during the nth period; τ_1^n is the initial entraining time when the outcrop line migration speed just catches up to the barotropic velocity; τ_2^n is the final entraining time when the outcrop line is overtaken by the barotropic velocity; that is,

$$v_B[f_0(t)] - \dot{f}_0(t)]|_{t=\tau_1^n,\tau_2^n} = 0;$$

and

$$\frac{d}{dt}[v_B(f_0) - \dot{f}_0]|_{t=\tau_1^n} > 0;$$

$$\frac{d}{dt}[v_B(f_0) - \dot{f}_0]|_{t=\tau_2^n} < 0. \tag{4.6b}$$

It is important to remember that the entraining stage defined here is independent of the structure of the solution because the subduction time in (3.7c) [or (4.2c)] is only determined by the $f$equation (3.7a) [or (4.2a)]. Now the physics for nonentrainment solution and entrainment solution as defined in (3.17) and (3.19) becomes clear. As stated in (4.5a,b), an entrainment solution has an entraining stage during which water is entrained into the mixed layer; a nonentrainment solution has no entraining stage and therefore water always subducts from the mixed layer into the thermocline.

Equation (4.5) can be written as constraints on the mixed-layer depth. Noticing (4.4a,b), we can rewrite (4.5a,b) as

$$-\frac{dH_m}{dt} > w_m \quad \text{when}$$

$$v_B(f_0) - \dot{f}_0 < 0, \quad \text{(nonentraining)} \tag{4.7a}$$

$$-\frac{dH_m}{dt} < w_m \quad \text{when}$$

$$v_B(f_0) - \dot{f}_0 > 0, \quad \text{(entraining)}. \tag{4.7b}$$

With $w_m = (1 - H_m)w_e < 0$, (4.7a) says that outside the entraining stage the mixed-layer depth either descends slowly or ascends at an arbitrary speed. Equation (4.7b) states that during the entraining stage the mixed layer must penetrate rapidly (faster than the downward particle speed). Considering that the dynamics of the present mixed layer differs significantly from that of a 1D model (e.g., Kraus and Turner 1967; Turner and Kraus 1967), it is interesting to see that the behavior of the mixed layer required by (4.7) is qualitatively consistent with that of a seasonal thermocline predicted from a 1D model. For example, a sharp rise of the mixed layer during the heating season is allowed in (4.7a); a strong penetration during the cooling season is required by (4.7b).

2) A CONVECTION SCHEME: DETERMINING THE MIXED-LAYER DEPTH DURING THE ENTRAINING STAGE

At first sight, the stable slope (3.14a) [or (4.5) or (4.7)] appears to guarantee a physical solution, but it does not! The problem arises during an entraining stage (4.6a). The outcrop line then moves southward faster than the particle. The waters subducted during this stage [with $t = \tau$ satisfying (4.6a)] are always left behind the outcrop line, no matter if (3.14a) is satisfied or not. [Note that (4.6) is independent of the solution structure.] This water mass would create gravitational instability in the water column north of the outcrop line (see the schematic example in Fig. 3d). To overcome the instability, physically, we should have a scheme to allow the unstable part of water to be entrained into the mixed layer. Here, we adopt a convective scheme that simply cuts off this part of unstable water. This scheme is illustrated schematically in Fig. 7, where the adjustment time interval Δt is assumed to be finite. After each time step, an unstable "bulb" is produced if the mixed-layer depth is not proper (say, if it were to remain unchanged). Then, we lower the mixed layer to the stable part of the thermocline at the latitude of the outcrop line. The unstable "bulb" is then cut off and is no longer a part of our solution. Physically, after this "bulb" is entrained into the mixed layer, it is well mixed within the mixed layer and can no longer be

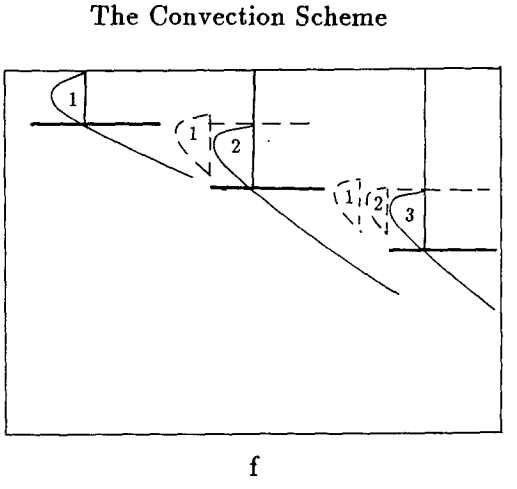

FIG. 7. The schematic figure of the convective scheme with a finite adjustment time interval. After each time, if the mixed layer remains unchanged, a bulb of unstable water is produced. Our convection scheme will allow the mixed layer to descend under the outcrop line such that the bulb is cut off.

identified as an entity. In other words, after the entrainment, the unstable part of water loses memory of its subduction time because it is well mixed with waters subducted at other times. If the time step becomes infinitesimal, these unstable bulbs will be squeezed, each having a zero volume. Consequently, our solution will have no unstable volume at any time. One should notice that this convective scheme is somewhat artificial. It says that the mixed layer entrains from below without changing its density (or the outcrop line). In our model, we are forced to do so because our outcrop line is specified and therefore cannot be altered.

The key for the scheme is, at any entrainment time t, to find the stable thermocline depth below the outcrop line. Then, we lower the new mixed layer to this depth. The water column under this thermocline must have subducted at a previous time, say, denoted by $\tau_p(t)(<t)$. From the subduction time $\tau(f, t)$ [in (3.7c) or (4.2c)], this corresponding $\tau_p(t)$ can be found as follows. During an entraining stage, north of the outcrop line, $\tau(f, t)$ has double values: a later subduction time at the branch $\tau^+(f, t)$ and an earlier one at the branch $\tau^-(f, t)$ [see Figs. 3c,d and discussion after (3.18) and (3.19)]. In particular, at the outcrop line $f_0(t)$, $\tau^+(f_0, t) \equiv t$ gives the present subduction time, while

$$\tau_p(t) \equiv \tau^-[f_0(t), t] \tag{4.8}$$

yields the corresponding previous subduction time, at which the injected water now arrives at $f_0(t)$. This τ_p mapping is shown schematically in Fig. 3c. By virtue of (4.8), the stable thermocline depth with the subduction time $\tau_p(t)$ is found from (4.2b) as $h^*[t, \tau_p(t)]$ (see Fig. 3d). Hence, our convective scheme requires a mixed-layer depth:

$$\boxed{H_m(t) = h^*[t, \tau_p(t)]} \quad \textit{during entraining stages.} \tag{4.9a}$$

Outside the entraining stage, this convection scheme does not impose any constraint on the mixed-layer depth. Thus, the stable slope (3.14a) still needs to be satisfied, or

$$\boxed{H_m(t) = \hat{H}_m(t)} \quad \textit{outside entraining stages.} \tag{4.9b}$$

Here $\hat{H}_m$ satisfies (4.7a). All the corresponding previous subduction times $\tau_p(t)$ such that t is during an entraining stage ($\tau_1^n \leqslant t \leqslant \tau_2^n$) form a new stage during which all the subducted waters will be reentrained in the following entraining stage (τ_1^n, τ_2^n). In other words, waters subducted during the new stage only establish the seasonal thermocline and can never enter the permanent thermocline as an identifiable entity. This stage is therefore called *the seasonally subducting stage.* The first entraining time τ_1^n entrains the water just subducted or $\tau_p(\tau_1^n) = \tau_1^n$, while the last entraining time τ_2^n entrains the earliest seasonally subducting water at the time

$$\tau_0^n \equiv \tau_p(\tau_2^n). \tag{4.10}$$

Hence, we have

$$\textit{seasonally subducting stage:} \quad \tau_0^n \leqslant t \leqslant \tau_1^n. \tag{4.11}$$

In contrast, waters subducted earlier than the seasonally subducting stage will never be entrained by the mixed layer and therefore enter the permanent thermocline. This stage is called *the permanently subducting stage* or simply *subducting stage,* which is represented as

$$\textit{subducting stage:} \quad \tau_2^{n-1} \leqslant t \leqslant \tau_0^n. \tag{4.12}$$

It is the waters subducted during this stage that create the permanent thermocline. Consequently, the variability in the permanent thermocline is completely determined by waters subducted during the subducting stage. Like the entraining stage, the subducting and seasonally subducting stages are also independent of the solution h because they are ultimately determined only by the f solution (4.2a).

As a result, one period can be divided into three stages: the seasonally subducting stage, the entraining stage, and the subducting stage. The waters injected during the seasonally subducting stage will be reentrained during the following entraining stage. In contrast, the waters subducted during the subducting stage provide water mass for the permanent thermocline. The mixed-layer depth during both the subducting and seasonally subducting stages must satisfy the stable slope condition (4.7a), which then, together with the convective scheme (4.9a), yields the mixed-layer depth during the following entraining stage.

3) A SCHEMATIC EXAMPLE: HOW TO DETERMINE THE SOLUTION

To have a better understanding of the physics of the three stages and the convective scheme, we investigate the thermocline evolution during one period as shown schematically in Fig. 8. Outside the entraining stage in (4.9b), we take

$$\hat{H}_m(t) = H_{\min} = \text{const},$$

$$\textit{subducting and seasonally subducting stages,} \tag{4.13}$$

which obviously satisfies a stable slope or (4.7a). Figure 8a shows some snapshots of the subduction time τ in (4.2c) as a function of f (similar to Fig. 3a), while the corresponding sections of h^* are depicted in Fig. 8b. The dashed lines, dotted lines, and solid lines, respectively, represent the part of τ and h^* for waters subducting during the seasonally subducting stage, the entraining stage, and the subducting stage. These stages are marked on the time axis in Figs. 8a,c,e. Since we concentrate on the nth period, only the part after τ_2^{n-1} will be considered as drawn in Figs. 8a,c,e. We start with Figs. 8a,b. Curve 1 occurs at September and consists of waters from the $(n-1)$th subducting stage

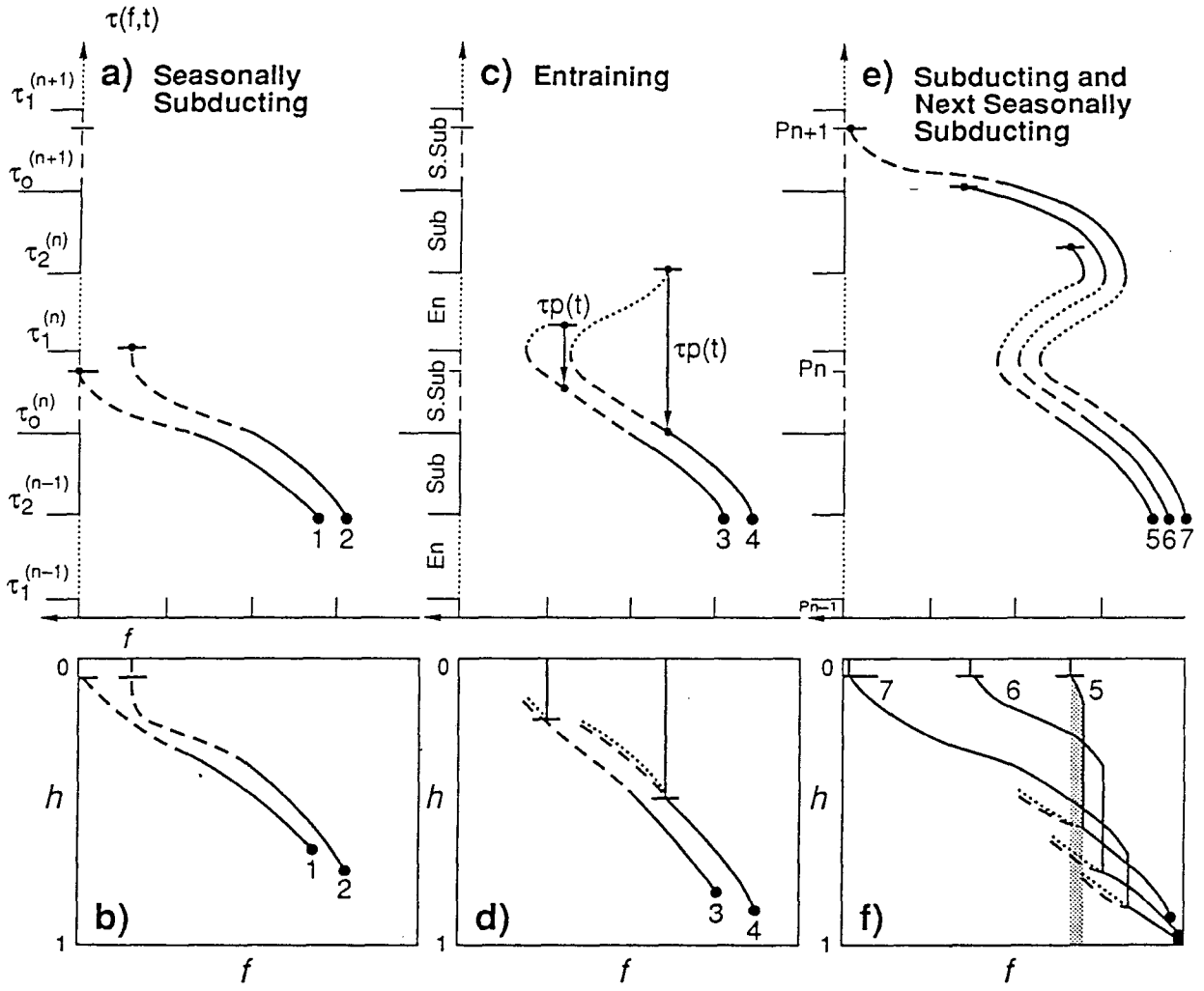

FIG. 8. The schematic figure of showing how to determine an entrainment solution in one cycle. The seasonally subducting stage, entraining stage, and subducting stage are drawn in dashed lines, dotted lines, and solid lines, respectively. (a), (c), and (e) The subduction time τ as a function of latitude f at different times in three stages. The times for different stages are also marked on the τ axis in (a), (c), and (e). (b), (d), and (f). The h^* profiles corresponding to (a), (c), and (e). After one cycle, a big pulse of water is subducted into the thermocline, part of which will be reentrained during the next entraining stage. (See the text for a full discussion.)

and part of the $(n-1)$th seasonally subducting stage. Similar to Figs. 3a,b, τ increases monotonically northward. This reflects the fact that during the seasonally subducting stage and subducting stage no water column will be overtaken by later subducting waters. Correspondingly, the h^* profile is stable. Curve 2 is at the last moment of the seasonally subducting stage and is qualitatively the same as curve 1 except that curve 2 is south of curve 1 at each subduction time τ, reflecting the southward advection due to $v_B < 0$. Since the mixed layer remains at $\hat{H}_m = H_{\min}$ according to (4.13), (4.7a) or (4.5a) says that there is no entrainment so far.

Figures 8c,d show time sections during the following entraining stage and therefore are similar to Figs. 3c,d. Curve 3 is at a time during the entraining stage. Part of the τ profile has been left north of the outcrop line, because during the $(n-1)$th entraining stage the outcrop line advances southward faster than the particles. According to our convective scheme (4.9a), the mixed-layer depth is deepened to the thermocline depth, which has developed from the water subducted at the corresponding seasonally subducting water at $\tau_p(t)$. Since this convection scheme is carried out from the first entraining time with an infinitesimal time interval, the unstable "bulb" is squeezed such that the unstable "bulb" has a zero volume, as opposed to a finite volume in Fig. 7. Curve 4 occurs at the last entraining moment τ_2^n, and the mixed layer has captured all the water injected during the entire previous seasonally subducting stage. The mixed layer now achieves its deepest depth.

In the following time, the subducting stage starts as shown in Figs. 8e, f. Curve 5 is at the time when the

outcrop line reaches the southernmost position. South of the outcrop line, a small pulse of water (the water column shaded in Fig. 8f) is seen subducted south of the outcrop line and under the mixed layer. This occurs because these waters are subducted after the last entraining time and thus move southward faster than the outcrop line. This pulse of waters will not be captured during the following entraining stage because the outcrop line now is moving northward and it will return after another period. The mixed layer suddenly (or discontinuously) rises from its deepest depth to its shallowest depth $H_{\min}$ due to (4.13). This abrupt ascent of H_m in turn produces a sharp jump of the interface in front of the subducted water pulse. Curves 6 and 7 occur, respectively, at the last subducting time and the next September with more waters subducted while the mixed layer remains unchanged due to (4.13). One cycle is completed.

b. *Entrainment solutions*

To see how the convective scheme overcomes instability, we present two examples of entrainment solutions with the outcrop lines used in the two unstable examples in Fig. 6. To simulate the rapid rise of a mixed layer during early spring more realistically, instead of using (4.13), we will adopt a parabolically ascending mixed layer during the subducting stage. Thus,

$$\hat{H}_m(t) = H_{\min} = \text{const} \quad \textit{seasonally subducting stage} \tag{4.14a}$$

$$\hat{H}_m(t) = H_m(\tau_2^n) - [H_m(\tau_2^n) - H_{\min}]\left(\frac{t - \tau_2^n}{\tau_0^{n+1} - \tau_2^n}\right)^{1/2} \quad \textit{subducting stage.} \tag{4.14b}$$

The minimum mixed-layer depth is set to be $H_{\min} = 0.1$—that is, one-tenth of the total depth. The mixed layer is then determined by (4.9a,b) and (4.14). Figure 9 presents an example under a strong decadal forcing $\omega = 5$, $a = 0.4$ (the same as in Figs. 6a–d). Figures 9a–d show the meridional sections in four "seasons." Solid lines are the physical solutions, while dotted lines are the unstable part (with zero volume) of the solution after the use of the convection scheme (4.9a). In September (Fig. 9a), the mixed-layer depth is at its minimum. During the following cooling season, the outcrop line accelerates southward and soon catches up with fluid particles. In December (Fig. 9b), the entraining stage has occurred for a rather long time and part of the seasonally subducted waters have been reentrained into the mixed layer (the newly formed dotted line). In March (Fig. 9c), the outcrop line arrives at the southernmost position. The entraining stage has finished and the subducting stage has started for a while. More waters have been reentrained into the mixed layer. In addition, a small amount of water (barely seen in the figure; the counterpart in the schematic example of Fig. 8 is the water column shaded in Fig. 8f) has subducted south of f_0 below the mixed layer and will never be caught by the outcrop line. In June (Fig. 9d), a big pulse of subducted water is formed partly because of the subduction left behind by the northward-moving outcrop line and partly because of the southward advection of the already subducted water. In this way a big pulse of water, which is mainly formed during the rather long subducting stage, is injected into the permanent thermocline. This big pulse of water is advected southward and downward. Later, part of the water will be reentrained in the next entraining stage (τ_1^{n+1}, τ_2^{n+1}) (not drawn in the figure).

The evolution of the mixed-layer depth and subduction potential vorticity $q_s = f_0/[1 - H_m(t)]$ are shown in Fig. 9f. In the figure, the H_m in the subducting stage is given by (4.14b); the H_m in the seasonally subducting stage (later than τ_0^{n+1} and before τ_1^n) is taken from (4.14a); and the H_m in the entraining stage is given by the convection scheme (4.9a). The potential vorticity shown in Fig. 9f indicates that the water subducted during the subducting stage has a lower potential vorticity while the water entrained into the mixed layer has a higher potential vorticity. Physically, this occurs because the subducted water comes from the mixed layer where water mass is well mixed and has a small potential vorticity. In contrast, the entrained water comes from the water that was heated during the seasonally subducting season with a strong stratification. Therefore, the seasonal thermocline acts as a source of low potential vorticity to the permanent thermocline in the subducting stage but as a sink of higher potential vorticity waters during the entraining stage (Woods 1985).

Figure 9e compares the time-mean solution (dot-connected lines) with two steady LPS thermocline solutions. The first steady thermocline is obtained by the time-mean outcrop line and mixed-layer depth (short dash line), while the second steady thermocline has its outcrop line and mixed layer at earlier "spring" [more precisely, at the time τ_2^n when the mixed layer reaches the deepest (long dash line)]. It is seen that the time-mean profile is close to the steady thermocline with the early "spring" outcrop line and mixed-layer depth. This phenomenon has been suggested by Stommel (1979). This is in sharp contrast to the nonentrainment solution if one compares the present Fig. 9e with Fig. 4e, where the time-mean theremocline is close to the steady thermocline with the time-mean outcrop line.

A local variation of the interface in the permanent thermocline (south of $f_{0\,\min}$) is shown in Fig. 9g. Similar to the nonentrainment solution in Fig. 4f, the interface deepens slowly and rises abruptly, although the outcrop line (3.13) is harmonic. The oscillation is somewhat close to the local depth of the steady thermocline with the "winter" mixed layer (long dashed line).

If the forcing frequency is increased, the speed of f_0 increases. But v_B is still the same. Thus, f_0 catches up

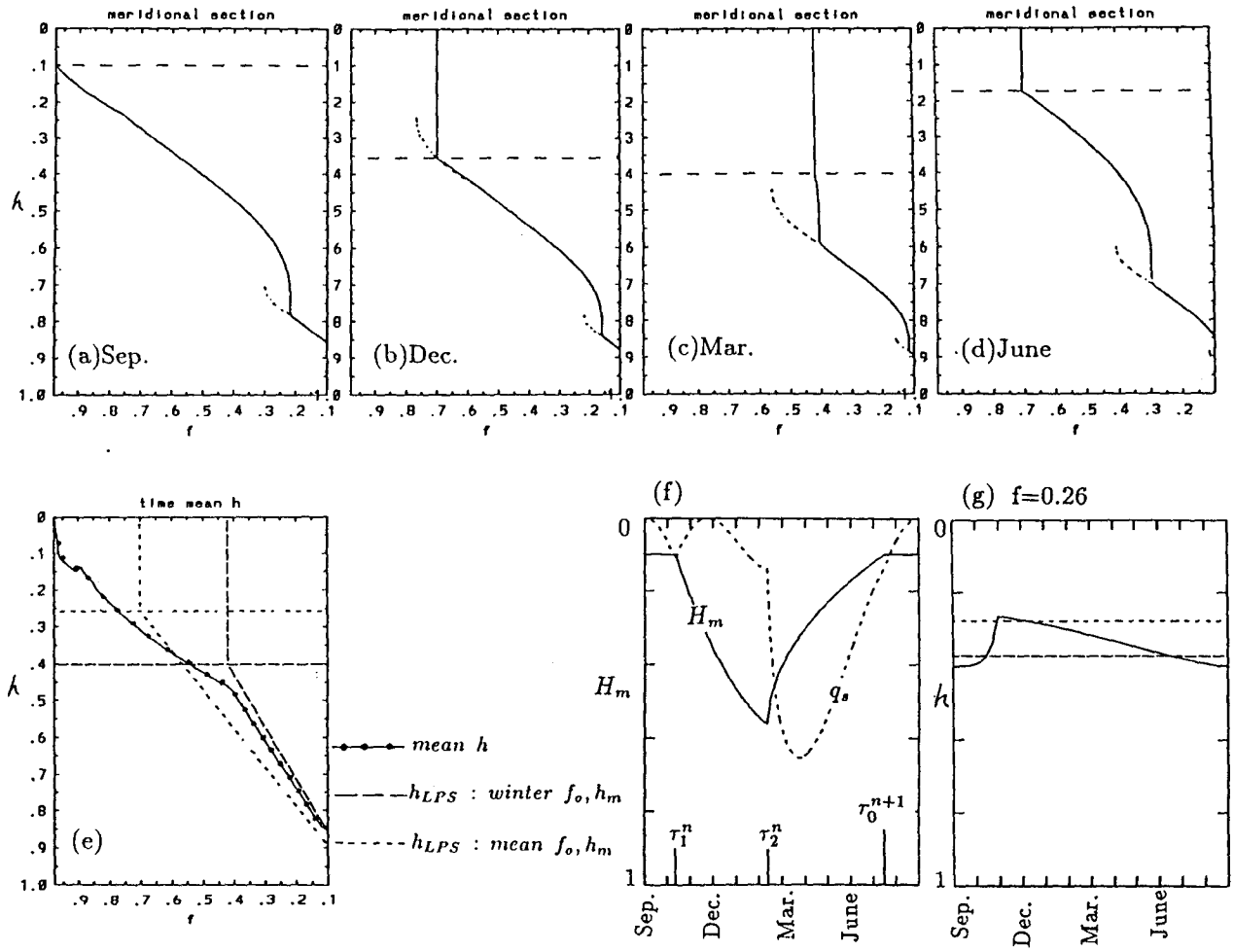

FIG. 9. Entrainment solution with a strong decadal forcing $\omega = 5$, $a = 0.4$ (the same as in Figs. 6a–d), and $H_{\min} = 0.1$. (a–d) Instantaneous sections at four seasons. (e) The time-mean profile (dot-connected line), the steady thermocline with the time-mean outcrop line and mixed-layer depth (short dashed line), and the steady thermocline with the outcrop line and mixed layer at winter (actually the last entraining time τ_2), when the mixed layer reaches the deepest. (f) Time series of the mixed-layer depth according to (4.14) outside the entraining stage and (4.9a) during the entraining stage. Subduction potential vorticity $q = f_0(t)/(1 - H_m(t))$ is also shown with a relative scale. (g) The local interface time series with the short and long dashed line being the steady thermocline with the time-mean and later winter (actually τ_2^n) f_0, H_m, respectively. In (f) and (g), the entraining and subducting stages are marked on the time axis.

with v_B sooner after September, and the entraining stage is elongated. As a result, more subducted water will be entrained into the thermocline and less water is left to subduct into the permanent thermocline. This is shown in Fig. 10 with an annual frequency forcing [$\omega = 50$, $a = 0.4$ in (3.13)] (same as Figs. 6e–h). Qualitatively, Fig. 10 is similar to the lower frequency case in Fig. 9. However, there are some important quantitative differences. First, as we expect, with a much higher frequency, much more subducted water is reentrained into the mixed layer (the dotted lines in Figs. 10a–d). Each year, only a small pulse of water subducts into the permanent thermocline, resulting in a very wavy permanent thermocline structure. Each wave pattern represents waters subducted during one subducting stage of one year. The smaller amount of subducted water than that in Fig. 9 is consistent with a much shorter subducting stage (about 1 month) (Fig. 10f) than that in Fig. 9f (about 5 months). (Here we compare the relative time normalized by the period.) Second, Fig. 10e shows that the time-mean thermocline almost coincides with the steady thermocline with the winter f_0 and H_m (actually at τ_2^n, which is almost March). In Fig. 10g, we also see that the thermocline oscillates very closely around the steady thermocline with the winter f_0 and H_m. All these suggest that for a higher frequency Stommel's (1979) conjecture becomes more correct. Last, Fig. 10g shows that the thermocline variability in this annual forcing case is much weaker than that in the decadal forcing case in Fig. 9g.

Finally, it should be pointed out that the shadow zone thermocline behavior should be similar to that

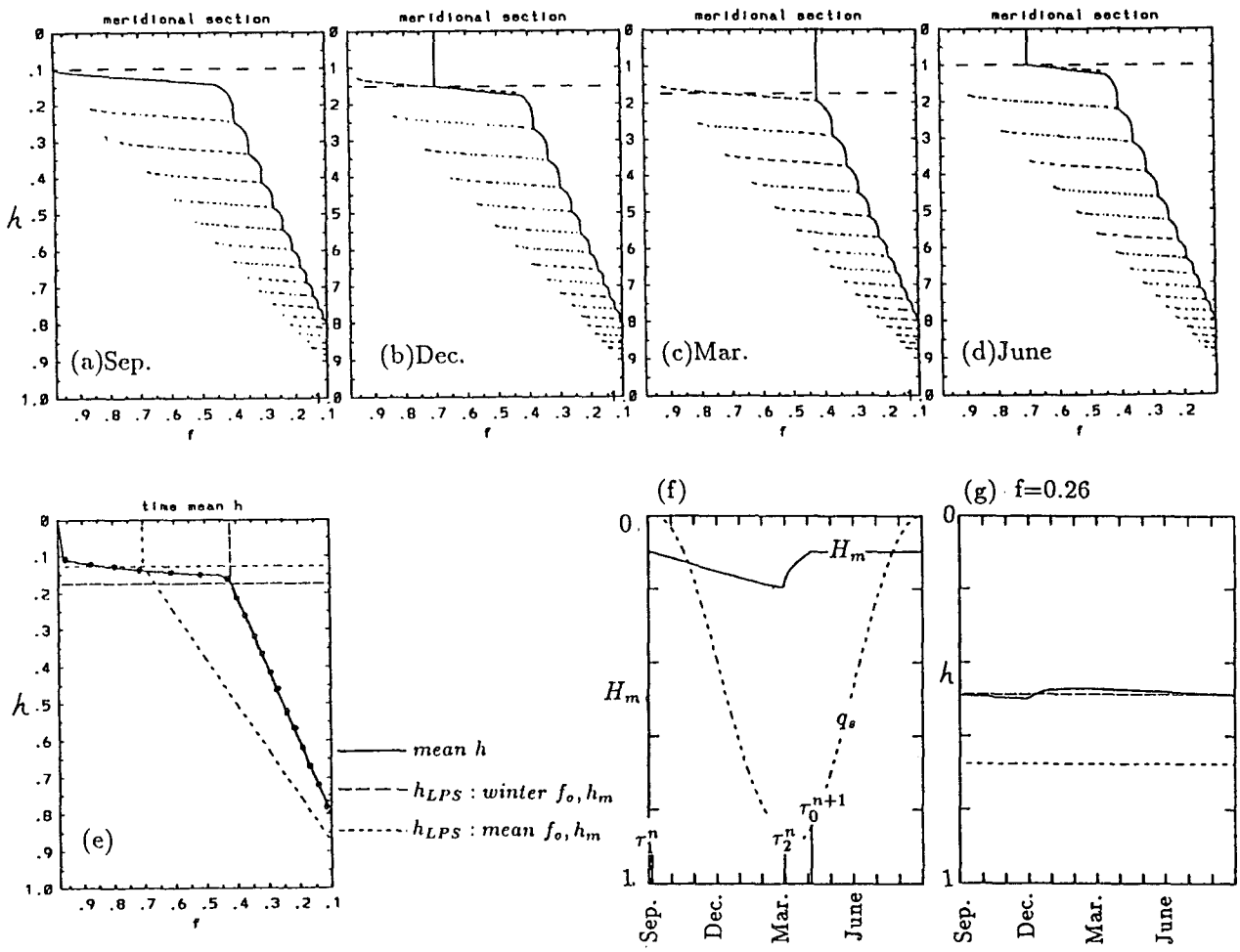

FIG. 10. Entrainment solution with a strong annual forcing $\omega = 50$, $a = 0.4$ (as in Figs. 6e–h). Other aspects are the same as Fig. 9. Compared with the decadal forcing case in Fig. 9. The synoptical profiles in (a–d) are much more wavy, implying a much smaller pulse of waters subducted into the permanent thermocline each year. The subducting stage (τ_1^n, τ_2^n) seen from Fig. 10f is much shorter than the decadal forcing case in Fig. 9f. The time-mean thermocline in (e) almost coincides with the steady thermocline with the winter mixed layer. The thermocline variability is much smaller in (g) than in Fig. 9g.

in the nonentrainment solution case. That is, the thermocline remains unchanged except in the western flank of the shadow zone where $x_B(f, t)$ sweeps through (as in Fig. 4 and Fig. 5).

5. Thermocline variability due to varying surface temperature

Now we come to our central issue: What is the thermocline variability in response to a varying surface buoyancy flux or a moving outcrop line? Since our model is not fully coupled, there are an infinite number of solutions. We will choose the solution with the mixed-layer depth specified by (4.14) because this mixed-layer depth variation seems to resemble the observations well as seen in Fig. 9f and Fig. 10f (at least for the annual frequency case—see, for instance, Kraus and Turner 1967; Turner and Kraus 1967).

The magnitude of local variability can be easily derived in terms of potential vorticity because of the fixed bottom in our model. In fact, $q = f/(1 - h)$ immediately gives $h(f, t_1) - h(f, t_2) = -f[1/q(f, t_2) - 1/q(f, t_1)]$. Hereafter, we concentrate on the permanent thermocline,[1] which is located south of the southernmost outcrop line latitude

$$f_{0\,\min} = \min[f_0(t)]. \tag{5.1}$$

[1] The permanent thermocline should be the region where the potential vorticity of each water column is always conserved. This requires that the water particle is not exposed to the mixed layer. Hence, in our model, the permanent thermocline will refer to the region south of the southernmost position of the outcrop line $f < f_{0\,\min} = \min\{f_0\}$—that is, where the potential vorticity of a layer 2 water column is conserved. In contrast, north of $f_{0\,\min}$, as a water column moves, its potential vorticity will be changed by the variation of the mixed-layer depth.

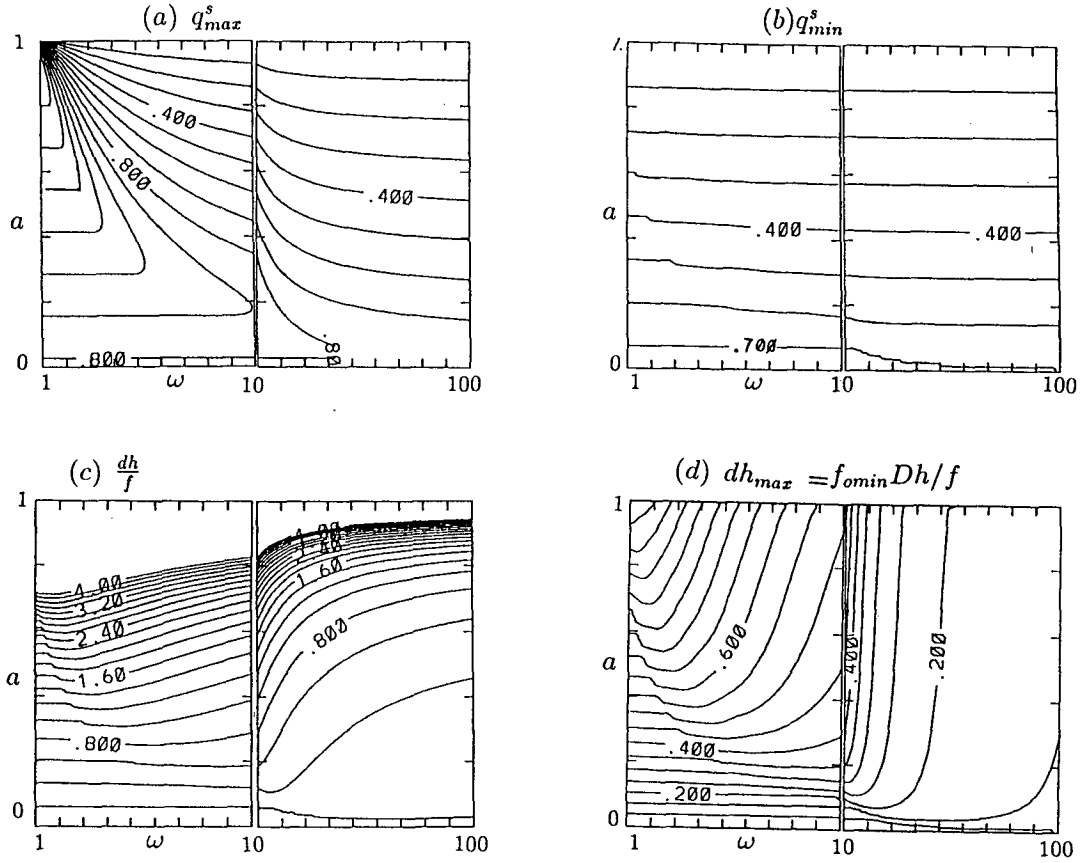

FIG. 11. The maximum and minimum subduction potential vorticity during the subducting stage $q^s_{\max}$, $q^s_{\min}$, the upper bound of local variability in the permanent thermocline $Dh/f = 1/q^s_{\min} - q^s_{\max}$, and the maximum variability in the permanent thermocline $dh_{\max} = f_g(1-a)(1/q^s_{\min} - q^s_{\max})$. We have chosen $f_g = 0.7$, $w_e(f) = -1$. The mixed layer varies according to (4.9) and (4.14).

The potential vorticity is conserved in the permanent thermocline and is therefore determined by waters subducted *during the subducting stage.* Therefore, the magnitude of variability in the permanent thermocline is

$$dh \leq Dh \equiv f\left[\frac{1}{q^s_{\min}} - \frac{1}{q^s_{\max}}\right], \qquad (5.2)$$

where $q^s_{\min}$ and $q^s_{\max}$ are minimum and maximum subduction potential vorticities $q^s = f_0/(1-H_m)$ *during the subducting stage.* Equation (5.2) suggests that the variability decreases with latitude. This occurs because at lower latitudes there is less planetary vorticity available to alter the stratification. In addition, the variability depends on the difference of subducted potential vorticities. Thus, a uniform potential vorticity in the permanent thermocline produces no thermocline variability.[2]

[2] This conclusion holds exactly in the rigid and flat-bottom model here. If the bottom varies with time, even with a uniform potential vorticity, thermocline variability may exist.

Using the outcrop line in (3.13) and the mixed-layer depth according to (4.9) and (4.14), with respect to the forcing amplitude a and frequency ω, we have calculated $q^s_{\max}$, $q^s_{\min}$, and $Dh/f = 1/q^s_{\min} - 1/q^s_{\max}$ in Figs. 11a–c, respectively. First of all, in the parametric plane (ω, a), one sees a critical boundary separating the slow outcrop line regime (small frequency or amplitude) from the fast outcrop line regime. This is the criterion dividing the nonentrainment solution (3.17) from the entrainment solution (3.19) (i.e., these ω, a make $v_B - f_0$ just realizable at a single time). In the nonentrainment regime, $q^s_{\max}$, $q^s_{\min}$, and Dh/f are independent of frequency because nonentrainment solutions have neither an entraining stage nor a seasonally subducting stage. Thus, the maximum and minimum subduction potential vorticities during the subducting stage are also those in the whole cycle; that is,

$$q^s_{\max} = q_{\max} = \frac{f_{0\max}}{1 - H_{\min}} = \frac{f_g(1+a)}{1 - H_{\min}},$$

$$q^s_{\min} = q_{\min} = \frac{f_{0\min}}{1 - H_{\min}} = \frac{f_g(1-a)}{1 - H_{\min}}. \qquad (5.3)$$

where (3.13a,b) have been used. Therefore, both $q^s_{\max}$ and $q^s_{\min}$ are independent of frequency. The variability, which results in (5.2), is also independent of frequency. In contrast, the variability for most of the entrainment solutions (in Fig. 11c) decreases with an increasing frequency. This gives another important difference between the thermocline variability of nonentrainment and entrainment solutions.

It can also be seen in Fig. 11b that, even in the entrainment regime, the minimum subduction potential vorticity $q^s_{\min}$ depends very weakly on frequency. In fact, if we use (4.13) in the subducting stage to replace (4.14b), we can show easily that $q^s_{\min}$ is the same as in (5.3) and is independent of frequency. Therefore, the frequency dependency of the variability Dh is mainly caused by $q^s_{\max}$. Roughly speaking, this is so because for different frequency $q^s_{\min}$ usually occurs during March but $q^s_{\max}$ varies at very different times. Thus, the planetary vorticity for $q^s_{\max}$ changes greatly with frequency.

Consider now the thermocline variability. The local variability at a latitude f can be derived by multiplying the values in Fig. 11c by f. It is seen that toward both high and low frequencies, the variability tends to be independent of frequency. But, in the transition regime between nonentrainment solutions and entrainment solutions (actually, this is the part of entrainment solutions near the nonentrainment solution), the variability (first increases slightly and then) decreases rapidly toward high frequencies. On the other hand, the frequencies for this transition regime usually occur for about decadal frequencies ($\omega \sim 10$) unless the forcing amplitude a is very large (say, $a > 0.5$) or very small (say, $a < 0.05$). Thus, we conclude that decadal forcing is the most efficient in forcing variabilities in the ventilated zone. This feature differs substantially from the wind forcing case discussed by Liu (1993b), especially at high frequencies. There, Liu showed that at high frequencies the response tends to be linear; that is, $Dh \sim a/\omega$, where the strongest frequency dependency of the variability also occurs.

Finally, one should be cautious in using Fig. 11c because at each different amplitude a the range of f for the permanent thermocline is different. In fact, the northern bound of the permanent thermocline is the southernmost outcrop latitude (5.1) [noting (3.13a,b)],

$$f_{0\min} = f_g(1 - a). \tag{5.4}$$

For a larger amplitude a, the possible $f_{0\min}$ decreases. As $a \to 1$, the minimum potential vorticity in (5.3) approaches zero. Thus, although the variability in Fig. 11c approaches infinity near $a = 1$, this infinity can never be achieved because then there is no permanent thermocline region; that is, $f_{0\min} = 0$. We can calculate the maximum variability within the whole permanent thermocline [actually at latitude $f = f_g(1 - a)$] with different forcings as

$$dh_{\max} = f_g(1 - a) \times Dh/f. \tag{5.5}$$

The results are plotted in Fig. 11d. The most striking feature is that at higher frequencies the maximum variability approaches a finite value at strong amplitude ($a \to 1$). Above decadal frequency, the maximum variability is almost amplitude independent and decreases with an increasing frequency. Therefore, toward high frequency, no matter how strong the forcing is the maximum variability tends to decrease rapidly. This is in sharp contrast with the lower-frequency case when the maximum variability is almost frequency independent. Thus, $Dh_{\max}$ is insensitive to frequency at lower frequency but decreases rapidly with frequency at high frequency. Alternatively, this fact suggests that a decadal buoyancy forcing (in the transition regime) is the most efficient in producing variability in the permanent thermocline.

6. Summary and discussion

The effect of annual and decadal varying surface temperature on the thermocline is examined in a simple model including an essentially passive mixed layer and two ideal fluid layers. The outcrop line is specified during the whole cycle while the mixed-layer depth is specified only during part of the cycle. Some important results are found. First of all, the surface buoyancy flux causes strong variability in the ventilated zone while it affects the shadow zone very little. In addition, it does not change the barotropic circulation. These are in sharp contrast to the case in which the Ekman pumping varies. In that case, it has been pointed out (Liu 1993a,b) that isopycnals of the thermocline exhibit strong variability in the shadow zone while they have little variability in the ventilated zone. At the same time, the circulation changes barotropically over the entire basin. Physically, the shadow zone is mainly controlled by the local Ekman pumping and Rossby waves from the eastern boundary. They have different response time scales and therefore produce an imbalance after a changing wind. On the other hand, the ventilated zone is mainly controlled by the density advection of the subducted waters, which tends to cancel a varying Ekman pumping through a barotropic process while it helps a varying surface heat flux to excite thermocline variability.

Second, there are two types of buoyancy forced solutions: the nonentrainment solution and the entrainment solution. A nonentrainment solution occurs when the southward speed of an outcrop line is always slower than near-surface particle velocity, which takes place under a weak surface cooling. The surface cooling is mainly balanced by the horizontal advection in the permanent thermocline. The mixed-layer depth varies little and the mixed layer is never entrained. The time-mean profile is close to the steady thermocline with the time-mean outcrop line. The variability in the permanent thermocline is independent of frequency.

An entrainment solution occurs when the outcrop line moves southward faster than the particle during part of the period, when the horizontal advection in the permanent thermocline is no longer strong enough to balance the surface cooling. Deep cold convection must occur. The mixed layer penetrates rapidly such that water mass is entrained into the mixed layer through the bottom. The local variability of the permanent thermocline is most efficiently produced by decadal forcings. At annual frequency, there is very little water subducted into the permanent thermocline each year, causing weak variability. The time-mean thermocline resembles the steady thermocline with the early spring mixed layer.

Furthermore, for a nonentrainment solution, water always subducts into the permanent thermocline. However, for an entrainment solution, there are three stages during each period: the seasonally subducting stage, the entraining stage, and the subducting stage. Waters subducted during the seasonally subducting stage will be reentrained in the following entraining stage as high potential vorticity waters to form the seasonal thermocline. The waters subducted during the subducting stage have a lower potential vorticity and establish the permanent thermocline.

Finally, for both entrainment and nonentrainment solutions, under a harmonic surface temperature forcing, the local interface variation always presents a rapid rise and a slow descent, implying a fast destruction and slow buildup of the stratification.

For a clear comparison, the above properties of nonentrainment and entrainment solutions are listed in Table 1.

TABLE 1. The comparison between nonentrainment and entrainment solutions.

	Nonentrainment solutions	Entrainment solutions
Forcing	Weak cooling	Strong cooling
Dynamics	Advection ~ cooling	Advection + convection ~ cooling
Entrainment	Detraining ($w_m^* < 0$)	Entraining ($w_m^* < 0$) + detraining ($w_m^* > 0$)
$\rho_m(t)$ or $(f_0(t))$	$\dot{f}_0 > v_B$ all the time	$\dot{f}_0 > v_B$ sometimes
$h_m(t)$	Weak variation	Strong variation
Mean structure	$\langle h \rangle \approx h$ (mean f_0, h_m)	$\langle h \rangle \approx h$ (winter f_0, h_m)
Variability $(\delta h(t))$	Independent of ω	Strongly dependent on ω

So far, observations are too poor to allow a comprehensive comparison with the theory here. Nevertheless, the observations available seem to be consistent with the theory. One example is the 18°C mode water. It is believed to be formed mainly by subduction in response to strong surface cooling in the northwestern part of a subtropical gyre (McCartney 1982) and, therefore, it is a good example to test the theory about the effect of surface heat flux. Talley and Raymer (1982) found that the 18°C mode water in the North Atlantic does have small pulses of potential vorticity at the annual period. In addition, the mode water has been observed to be not very sensitive to the strong surface annual heat flux variation. Relatively significant changes arise at interannual time scales. These observations are in accordance with the theory here.

Perhaps an even more important phenomenon is the thermocline variability in the northern part of a subtropical gyre. Observations have indicated that the annual response in the northern part of the subtropical gyres in both the North Pacific and the North Atlantic is mainly barotropic while in the southern part the response is mainly baroclinic (Gill and Niiler 1973). Later, observations (Price and Magaard 1980, 1986; White and Saur 1983) found no signals and very weak signals of interannual baroclinic Rossby waves in the northern part of the subtropic gyre in the North Pacific and the North Atlantic, respectively. In contrast, in the southern parts of the subtropical gyres in both oceans, clear baroclinic Rossby wave signals are identified at annual and interannual frequencies.

These observations are consistent with the theory about the effect of a varying Ekman pumping as discussed by Liu (1993a,b). The thermocline in the northern part of a subtropical gyre is mainly occupied by a ventilated zone, where the advection from the subducted water tends to balance the local Ekman pumping. As a result, little baroclinic Rossby wave activity exists. On the contrary, the thermocline in the southern part of a subtropical gyre is mostly occupied by a shadow zone, where advection plays little role. Baroclinic Rossby waves and local Ekman pumping dominate the response. Consequently, the activity of baroclinic waves is strong. Therefore, the different dynamic balances in a ventilated zone and a shadow zone may offer an explanation for the lack of baroclinic signals in the northern parts of the subtropical gyres. When we consider the effect of a varying surface temperature, we find that at interannual time scales the variable surface heat flux is able to force strong baroclinic variability in the ventilated zone through the advection of the subducted waters from the mixed layer. This may suggest that the variability in the northern part of a subtropical gyre may be forced primarily by the surface heat flux through subduction rather than by the local Ekman pumping and Rossby waves.

In spite of the difficulty of observations, recent numerical experiments have provided encouraging results. Bleck et al. (1989) and Hu and Bleck (1992) studied the thermocline–mixed layer system using a numerical model in isopycnic coordinates. They have concentrated on annual periods so far. In general, their results agree with the present theory. For example, with a strong annual surface heat flux variation, the permanent thermocline in their model changes little although the seasonal thermocline varies dramatically. In ad-

dition, although the annual surface forcing varies harmonically, layer interfaces locally exhibit a faster shallowing and a slower deepening. Furthermore, at the annual time scale, the mixed-layer dynamics is determined mainly by local processes and therefore horizontal advection is not important. Much more detailed analysis is still needed to improve our understanding and compare with the theory. In particular, it would be important to examine results from numerical experiments at decadal time scales.

Much can be done to improve our present model. First, the mixed-layer model is not active. For a true understanding of the effect of a variable surface buoyancy flux on the thermocline, it is crucial to couple an active mixed layer with the permanent thermocline. Second, the vertical resolution needs to be improved. The flat bottom used here is artificial, because the thermocline bottom is neither rigid nor flat. The study of a coupled mixed layer and a two-and-a-half-layer ideal fluid thermocline model will be helpful in clarifying some artificial features of our flat bottom. The two-layer vertical resolution is too crude to resolve a poleward deepening mixed-layer bottom [as shown in (4.1)], which has been seen important in steady cases. At least three thermocline layers are needed to investigate the effect of a tilting mixed-layer bottom (Wang 1990; Pedlosky and Robbins 1991). In addition, as the layer number is increased, even with a zonal outcrop line, the thermocline in the ventilated zone should be dependent on Ekman pumping, while the thermocline in the shadow zone should be related to the outcrop line. [This can be seen in the steady cases with layered LPS model (Luyten et al. 1983) or the continuously stratified model (Huang 1986).] Therefore, the thermocline variability in both zones will be more complicated.

Acknowledgments. This is part of ZL's Ph.D. thesis completed in the Joint Program of MIT/Woods Hole Oceanographic Institution. ZL is grateful for many discussions with Drs. R. X. Huang, G. Flierl, C. Wunsch, and J. Price. ZL also thanks Drs. G. Flierl and P. Rizzoli for generously letting him use their Sun cluster computers. Useful suggestions and careful reading of the manuscript of D. Marshall are greatly appreciated. The suggestions of two reviewers were very helpful in clarifying the paper. This work is supported by the Division of Atmospheric Research, NSF.

APPENDIX

The Mathematical Derivation of $\partial_f h|_{f=f_0}$

Differentiating (4.2b) with respect to t_i yields

$$\partial_{t_i} h^* = \frac{1}{f_0^2} \times \left[f^* f_0 \frac{dH_m}{dt_i} - (1 - H_m)(f^*_{t_i} f_0 - \dot{f}_0 f^*) \right], \quad \text{(A.1)}$$

where $f^*_{t_i}$ is given in (3.18). Thus, with (3.18) and using $f_0 = f^*$ at $t_i = t$ and $v_B = fw_e$, we obtain

$$\partial_f h|_{f=f_0(t)} = \left.\frac{\partial_{t_i} h^*}{\partial_{t_i} f^*}\right|_{t_i=t} = \frac{(dH_m/dt_i) + w_e(f_0)(1 - H_m)}{-[v_B(f_0) - \dot{f}_0]}. \quad \text{(A.2)}$$

The entrainment velocity at the bottom of the mixed layer at the outcrop line is

$$w^*_m = \frac{dH_m}{dt} + w_m, \quad \text{(A.3)}$$

where $w_m = w|_{f=f_0, z=-H_m}$ is the vertical velocity at the bottom of the mixed layer under the outcrop line. This vertical velocity can be proven to be

$$w_m = (1 - H_m) w_e(f_0). \quad \text{(A.4)}$$

Indeed, since in (2.10) we assumed that the density in the mixed layer is zonally independent, the meridional velocity in the mixed layer is barotropic. Moreover, in (4.1) or the solution (4.2), we have adopted a zonal outcrop line and a zonally independent mixed-layer depth. Thus, in the ventilated zone, it holds that $\partial_x h = \partial_x h_m = \partial_x \gamma_m = 0$. Consequently, in all the layers, the meridional velocities are barotropic; that is, $v_m = v_1 = v_2 = v_B$. Integrating the vorticity equation of the mixed layer $v_m = fw_z$ from the bottom to the top of the mixed layer, we have $H_m v_B = H_m v_m = fw_e - fw(-H_m)$. Using the Sverdrup relation $v_B = fw_e$, we obtain (A.4). Equations (A.3) and (A.4) then give

$$w^*_m = \frac{dH_m}{dt} + (1 - H_m) w_e. \quad \text{(A.5)}$$

Thus, (A.2) becomes

$$\partial_f h|_{f=f_0} = \frac{w^*_m}{-[v_B(f_0) - \dot{f}_0]}. \quad \text{(A.6)}$$

REFERENCES

Anderson, D. L. T., and A. E. Gill, 1975: Spin-up of a stratified ocean, with applications to upwelling. *Deep-Sea Res.*, **22**, 583–596.

Bleck, R., H. P. Hanson, D. Hu, and E. B. Kraus, 1989: Mixed layer-thermocline interaction in a three-dimensional isopycnic coordinate model. *J. Phys. Oceanogr.*, **19**, 1417–1439.

Gill, A. E., and P. P. Niiler, 1973: The theory of the seasonal variability in the ocean. *Deep-Sea Res.*, **20**, 141–177.

——, and J. S. Turner, 1976: A comparison of seasonal thermocline models with observation. *Deep-Sea Res.*, **23**, 391–401.

Hu, D., and R. Bleck, 1993: A joint mixed-layer/isopycnic coordinate model of wind- and thermohaline-driven ocean general circulation. Part II: Results of the control run and thermocline ventilation. *J. Phys. Oceanogr.*, submitted.

Huang, R. X., 1986: Solutions of the ideal fluid thermocline with continuous stratification. *J. Phys. Oceanogr.*, **16**, 39–59.

——, 1989: The generalized eastern boundary conditions and the three-dimensional structure of the ideal fluid thermocline. *J. Geophys. Res.*, **94**, 4855–4865.

Kraus, E. B., and J. S. Turner, 1967: A one-dimensional model of the seasonal thermocline. II. The general theory and its consequences. *Tellus*, **19**, 98–105.

Levitus, S., 1982: *Climatological Atlas of the World Ocean.* NOAA Prof. Pap., No. 13, U.S. Govt. Printing Office, 173 pp.

Liu, Z., 1991: Time-dependent ventilated thermocline. Ph.D. thesis, Joint Program of MIT/Woods Hole Oceanographic Institution, 208 pp.

——, 1993a: Thermocline variability forced by varying Ekman pumping. Part I: Spinup and spindown. *J. Phys. Oceanogr.*, **23,** 2505–2522.

——, 1993b: Thermocline variability forced by varying Ekman pumping. Part II: Annual and decadal Ekman pumping. *J. Phys. Oceanogr.*, **23,** 2523–2540.

Luyten, J. R., J. Pedlosky, and H. Stommel, 1983: The ventilated thermocline. *J. Phys. Oceanogr.*, **13,** 292–309.

Marshall, J., and G. Nurser, 1991: A continuously stratified thermocline model incorporating a mixed layer of variable thickness and density. *J. Phys. Oceanogr.*, **21,** 1780–1792.

McCartney, M. S., 1982: The subtropical recirculation of Mode Waters. *J. Mar. Res.*, **40**(Suppl.), 427–464.

Niiler, P. P., and E. B. Kraus, 1977: One-dimensional models. *Modeling and Prediction of the Upper Layers of the Oceans.* E. B. Kraus, Ed., Pergamon, 143–172.

Pedlosky, J., and P. Robbins, 1991: The role of finite mixed-layer thickness in the structure of the ventilated thermocline. *J. Phys. Oceanogr.*, **21,** 1018–1031.

——, W. Smith, and J. R. Luyten, 1984: On the dynamics of the coupled mixed-layer-thermocline system and the determination of the oceanic surface density. *J. Phys. Oceanogr.*, **14,** 1159–1171.

Price, J. M., and L. Magaard, 1980: Rossby wave analysis of the baroclinic potential energy in the upper 500 meters of the North Pacific. *J. Mar. Res.*, **38,** 249–264.

——, and ——, 1986: Interannual baroclinic Rossby waves in the Mid-latitude North Atlantic. *J. Phys. Oceanogr.*, **16,** 2061–2070.

Stommel, H., 1979: Determination of watermass properties of water pumped down from the Ekman layer to the geostrophic flow below. *Proc. Natl. Acad. Sci. USA*, **76,** 3051–3055.

Talley, L. D., and M. E. Raymer, 1982: Eighteen degree water variability. *J. Mar. Res.*, **40**(Suppl), 757–775.

Turner, J. S., and E. B. Kraus, 1967: A one-dimensional model of the seasonal thermocline: I. A laboratory experiment and its interpretation. *Tellus*, **19,** 88–97.

Wang, L. P., 1990: The dynamical effect of the mixed-layer on the interior ideal fluid thermocline.

Warren, B. A., 1972: Insensibility of subtropical mode water characteristics to meteorological fluctuations. *Deep-Sea Res.*, **19,** 1–20.

White, W. B., and J. F. Saur, 1983: Sources of interannual baroclinic waves in the Eastern Subtropical North Pacific. *J. Phys. Oceanogr.*, **13,** 531–544.

Woods, J. D., 1985: Physics of thermocline ventilation. *Coupled Atmosphere–Ocean Models,* J. C. J. Nihoul, Ed., Elsevier.